

# The $Q_{weak}$ Experiment: A Search for New Physics at the TeV Scale Via a Measurement of the Proton's Weak Charge

December 3, 2001

D. Armstrong<sup>1</sup>, T. Averett<sup>1</sup>, J.D. Bowman<sup>5</sup>, R. Carlini<sup>9</sup> (contact person), C.A. Davis<sup>11</sup>, J. Erler<sup>3</sup>, R. Ent<sup>9</sup>, M. Finn<sup>1</sup>, T.A. Forest<sup>6</sup>, K. Johnston<sup>6</sup>, R. Jones<sup>2</sup>, S. Kowalski<sup>8</sup>, L. Lee<sup>7</sup>, A. Lung<sup>9</sup>, D. Mack<sup>9</sup>, S.A. Page<sup>7</sup>, S. Penttila<sup>5</sup>, M. Pitt<sup>10</sup>, M. Poelker<sup>9</sup>, W.D. Ramsay<sup>7</sup>, M. Ramsey-Musolf<sup>2,4</sup>, J. Roche<sup>1,9</sup>, N. Simicevic<sup>6</sup>, G. Smith<sup>9</sup>, R. Suleiman<sup>8</sup>, S. Taylor<sup>8</sup>, W.T.H. van Oers<sup>7</sup>, S. Wells<sup>6</sup>, S. Wilburn<sup>5</sup>, S.A. Wood<sup>9</sup>

<sup>1</sup>*College of William and Mary, Williamsburg, VA*

<sup>2</sup>*University of Connecticut, Storrs, Connecticut*

<sup>3</sup>*David Rittenhouse Laboratory, University of Pennsylvania, Philadelphia, Pennsylvania  
(New address (1/1/2002): Instituto de Fisica, Universidad Nacional Autonoma de Mexico,  
01000 Mexico D.F., Mexico)*

<sup>4</sup>*Kellogg Radiation Laboratory, California Institute of Technology, Pasadena, California*

<sup>5</sup>*Los Alamos National Laboratory, Los Alamos, New Mexico*

<sup>6</sup>*Louisiana Tech University, Ruston, Louisiana*

<sup>7</sup>*University of Manitoba, Winnipeg, Manitoba, Canada*

<sup>8</sup>*Massachusetts Institute of Technology, Cambridge, Massachusetts*

<sup>9</sup>*TJNAF, Newport News, VA*

<sup>10</sup>*Virginia Polytechnic Institute, Blacksburg, Virginia*

<sup>11</sup>*TRIUMF, Vancouver, Canada*

# Contents

<b>1</b>	<b>Introduction</b>	<b>3</b>
<b>2</b>	<b>Physics Motivation</b>	<b>5</b>
2.1	Running of $\sin^2 \theta_W$	5
2.2	Beyond the Standard Model	7
2.2.1	Model independent constraints	8
2.2.2	Extra neutral gauge interactions	9
2.2.3	Other models: supersymmetry and leptiquarks	11
2.2.4	Summary	12
2.3	Theoretical Interpretability	12
<b>3</b>	<b>The Experiment</b>	<b>15</b>
3.1	Spectrometer Magnet	15
3.1.1	Resistive coil geometry and cost estimate	18
3.1.2	Magnetic field calculations and optics	18
3.2	Detection	20
3.2.1	Rate estimate	20
3.2.2	Detectors	22
3.2.3	Electronics	23
3.3	Cryotarget	25
3.3.1	Refrigeration	25
3.3.2	Density variations	27
3.3.3	Cryotarget design and cost estimate	28
3.4	High Current Beam	30
3.4.1	Technical feasibility from the injector viewpoint	30
3.4.2	Miscellaneous administrative limits	30
3.5	Beam Polarimetry	31
3.5.1	University of Basel Møller polarimeter in Hall C	31
3.5.2	Compton polarimeter	32
3.6	Statistical Error and Random Noise	35
3.7	Systematic Errors	37
3.7.1	Corrections due to helicity-correlated beam properties	37
3.7.2	Determination of average $Q^2$	38
3.7.3	Nucleon form factor contributions	39
3.7.4	Effects due to transverse polarization	40
3.7.5	Null tests	41
3.8	Backgrounds	41
3.8.1	Backgrounds from target windows	41
3.8.2	Backgrounds from other reactions	43
3.8.3	Signal-to-background dilution factor	43
3.9	Total Error Budget	44

<b>4</b>	<b>Cost and Schedule</b>	<b>45</b>
<b>5</b>	<b>The Collaboration</b>	<b>46</b>
<b>6</b>	<b>Beam Request</b>	<b>46</b>
<b>7</b>	<b>Summary</b>	<b>46</b>
<b>A</b>	<b>The <math>G^0</math> Magnet Option</b>	<b>51</b>
<b>B</b>	<b>Physics Beyond the Standard Model</b>	<b>54</b>
	B.1 Extra Neutral Gauge Interactions . . . . .	55
	B.2 Supersymmetry . . . . .	57
	B.3 Leptoquarks . . . . .	58
<b>C</b>	<b>Miscellaneous Administrative Limits</b>	<b>62</b>
	C.1 Beam Dump Current Density Limit . . . . .	62
	C.2 Site Boundary Dose . . . . .	62
	C.3 Beam Containment Policy Current Limit . . . . .	63
	C.4 Physics Division Administrative Limit . . . . .	64
<b>D</b>	<b>Window Backgrounds</b>	<b>65</b>

## Abstract

We propose a new precision measurement of parity violating electron scattering on the proton at very low  $Q^2$  and forward angles to challenge predictions of the Standard Model and search for new physics. A unique opportunity exists to carry out the first precision measurement of the proton's weak charge,  $Q_W^p = 1 - 4\sin^2\theta_W$ , at JLab, building on technical advances that have been made in the laboratory's world-leading parity violation program and using the results of earlier experiments to constrain hadronic corrections. A 2200 hour measurement of the parity violating asymmetry in elastic  $ep$  scattering at  $Q^2 = 0.03 \text{ (GeV/c)}^2$  employing 180  $\mu\text{A}$  of 80% polarized beam on a 35 cm liquid Hydrogen target will determine the proton's weak charge with  $\simeq 4\%$  combined statistical and systematic errors. The Standard Model makes a firm prediction of  $Q_W^p$ , based on the running of the weak mixing angle  $\sin^2\theta_W$  from the  $Z^0$  pole down to low energies, corresponding to a  $10\sigma$  effect in our experiment. Any significant deviation of  $\sin^2\theta_W$  from the Standard Model prediction at low  $Q^2$  would be a signal of new physics, whereas agreement would place new and significant constraints on possible Standard Model extensions. In the absence of physics beyond the Standard Model, our experiment will provide a  $\simeq 0.3\%$  measurement of  $\sin^2\theta_W$ , making this a very competitive standalone measurement of the weak mixing angle.

## 1 Introduction

Precision tests have traditionally played a crucial role in elucidating the structure of the electroweak interaction. Measurements to date have provided an impressive array of constraints both on the Standard Model as well as on proposed scenarios for extending it. Measurements at the  $Z^0$  pole have constrained the weak mixing angle  $\sin^2\theta_W$  to impressive precision at that energy scale. However, a precision experimental study of the evolution of the weak mixing angle to lower energies has not yet successfully been carried out. The Standard Model evolution predicts a shift of  $\Delta\sin^2\theta_W = +0.007$  at low  $Q^2$  with respect to the  $Z^0$  pole best fit value of  $0.23113 \pm 0.00015$  (Figure 1). This shift corresponds to a 10 standard deviation effect in our proposed measurement, including both experimental and theoretical systematic errors. Any significant deviation of  $\sin^2\theta_W$  from the Standard Model prediction at low  $Q^2$  would be a signal of new physics, whereas agreement would place new and significant constraints on possible Standard Model extensions.

It must be stressed that there is an essential complementary between high energy studies at the  $Z^0$  pole in  $e^+e^-$  collisions and precision low energy tests, of which the proposed experiment is one. Small but perceptible deviations of a handful of low energy observables from their Standard Model predicted values are already beginning to provide new clues about the nature of physics that lies beyond. Hints of a deviation from the Standard Model evolution of  $\sin^2\theta_W$  may have been seen in atomic parity violation experiments which determine the weak charges of heavy nuclei, but a significant uncertainty in the theoretical interpretation severely limits the impact of the atomic physics results. In contrast, a precision measurement of the weak charge of the proton,  $Q_W^p = 1 - 4\sin^2\theta_W$ , proposed here at Jefferson Laboratory, addresses the same physics issues but is free of many-body theoretical uncertainties. The dominant hadronic effects that must be accounted for in extracting  $Q_W^p$  from the data are contained in form factor

contributions which can be sufficiently constrained by the current program of parity violating electron scattering measurements without reliance on theoretical nucleon structure calculations. This new experiment will be a crucial element of a program of very sensitive low energy tests of the Standard Model that is complementary to other efforts underway or planned world wide. Our proposed measurement is also complementary to SLAC experiment E158 which is carrying out parity violating asymmetry measurements in the purely leptonic sector at similar  $Q^2$ , but is currently not expected to reach a similar precision in  $\sin^2 \theta_W$ .

We will determine  $Q_W^p$  by measuring the parity violating asymmetry in elastic  $ep$  scattering at  $Q^2 = 0.03 \text{ (GeV/c)}^2$ . A toroidal magnetic field will focus elastically scattered electrons onto a set of 8 rectangular quartz Cerenkov detectors coupled to photomultiplier tubes which will be read out in current mode. The acceptance averaged asymmetry in our design is -0.28 ppm; we will measure this asymmetry to  $\pm 2.0\%$  statistical and  $\pm 2.0\%$  systematic errors in a 2200 hour measurement with 180  $\mu A$  of 80% polarized beam on a 35 cm liquid Hydrogen target. This measurement will determine the proton's weak charge with  $\simeq 4\%$  combined statistical and systematic errors, leading to a determination of  $\sin^2 \theta_W$  at the  $\pm 0.3\%$  level at low energy.

The experiment proposed here builds upon the world-leading parity violation program at Jefferson Lab. The current parity-violation experiments (HAPPEX, HAPPEX II, HAPPEX  $^4\text{He}$ , and  $G^0$ ) will provide high quality data on form factors that will be used to determine the contributions of hadronic structure to the proposed measurement. Unlike the other elements of this program, the  $Q_W^p$  experiment will constitute the first precision Standard Model test to be carried out at Jefferson Lab. Technical developments that are required for this experiment to proceed are relatively straightforward extensions of what has already been achieved with Jefferson Lab's world-leading polarized electron source or planned for future elements of the laboratory's parity program. The instrumentation design for the experiment is relatively simple, and we are confident that the experiment can be carried out to the stated precision goals.

This collaboration submitted a Letter of Intent (LOI-01-101) to the PAC in July 2001, and was encouraged to develop a proposal. The PAC report raised a number of issues which are addressed in the present document. Among these, it should be noted that key theorists continue to play a very active role in the collaboration, contributing to a sharpened physics case for the proposed measurement in the context of plausible competing theories for Standard Model extensions. An updated theory section is backed up by a lengthy Appendix in which predictions of alternate theories and implications for  $Q_W^p$  are explored. On the technical side, the collaboration has adopted a conservative, room temperature magnet design, is working on plans to implement an on-line Compton Polarimeter in Hall C, has resolved most issues associated with high current beam delivery for the experiment, and has arrived at an innovative and cost-effective solution for the required target cooling power.

Finally, we note that the new NSAC Long Range Plan has identified the search for physics beyond the Standard Model as one of the five primary scientific goals for the field during the coming decade. Like the parity violating deep inelastic scattering experiment performed at SLAC in the 1970's which had such a major impact on the fields of nuclear and particle physics [1,2], the  $Q_W^p$  measurement proposed here could become Jefferson Laboratory's signature contribution to the quest for physics beyond the Standard Model. Upon approval by the PAC, the collaboration will pursue an aggressive schedule for funding and equipment construction, with the goal of

taking first data in approximately 4 years' time.

## 2 Physics Motivation

The Standard Model (SM) of electroweak interactions has been confirmed with impressive precision in a variety of experiments, ranging in energies from the eV scale in atomic parity violation to a few hundred GeV in collisions at HERA, LEP, SLC, and the Tevatron. Consequently, the attention of the particle physics community has turned from testing the SM and measuring its parameters to searching for possible physics which may lie beyond it. In addition to Higgs boson searches, the search for signatures of such “new” physics is one of the primary objectives of present and future high energy collider experiments.

### 2.1 Running of $\sin^2 \theta_W$

An essential, but not yet well-tested, prediction of the Standard Model is the variation of  $\sin^2 \theta_W$  with momentum transfer  $Q^2$ , referred to as the “running of  $\sin^2 \theta_W$ ”. Testing this prediction requires a set of precision measurements at a variety of  $Q^2$  points, with sufficiently small and well understood theoretical uncertainties associated with the extraction of  $\sin^2 \theta_W$ , that one can interpret the results with confidence. It clearly also requires a careful evaluation of the Standard Model radiative corrections to  $\sin^2 \theta_W$  in the context of the renormalization group evolution (RGE) of the gauge couplings. Such tests have been crucial in establishing QCD as the correct theory of the strong interaction [12], and the RGE evolution of the QED coupling has also been demonstrated experimentally [13]. However, the gauge coupling of the weak interaction, at low energies represented by the weak mixing angle  $\sin^2 \theta_W$ , has not yet been studied successfully in this respect.

Figure 1 shows the Standard Model prediction in a particular scheme<sup>1</sup> for  $\sin^2 \theta_W$  together with existing and proposed world data. As is seen from the figure, the very precise measurements near the  $Z^0$  pole merely set the overall magnitude of the curve; to test its shape one needs precise off-peak measurements. Currently there are only two off-peak measurements of  $\sin^2 \theta_W$  which test the running at a significant level: one from atomic parity violation (APV) and one from high energy neutrino-nucleus scattering (NuTeV). Our proposed measurement of  $Q_W^p$  will be performed with significantly smaller statistical and systematic errors and has a much cleaner theoretical interpretation than existing low  $Q^2$  data. It is complementary to, and will be carried out to higher precision than an approved experiment E-158 at SLAC which will attempt to determine  $\sin^2 \theta_W$  from parity violating  $\vec{e}e$  (Møller) scattering at low  $Q^2$  [4,5].

The importance of a new  $Q_W^p$  measurement is underlined by the current situation in atomic parity violation. To date, the most precise measurement of low-energy neutral current interactions has been carried out by exploiting parity-violating effects in Cesium, which allow a determination of the weak charge of the Cesium nucleus. Unfortunately, the reliability of this determination appears to be subject to considerable theoretical atomic structure uncertainties.

---

<sup>1</sup>Note that  $\sin^2 \theta_W$  is not strictly an observable, but depends on what has been absorbed into the definition and what has been corrected for. This graph shows a recent calculation by Erler and Ramsey-Musolf, details of which are given in Appendix B.

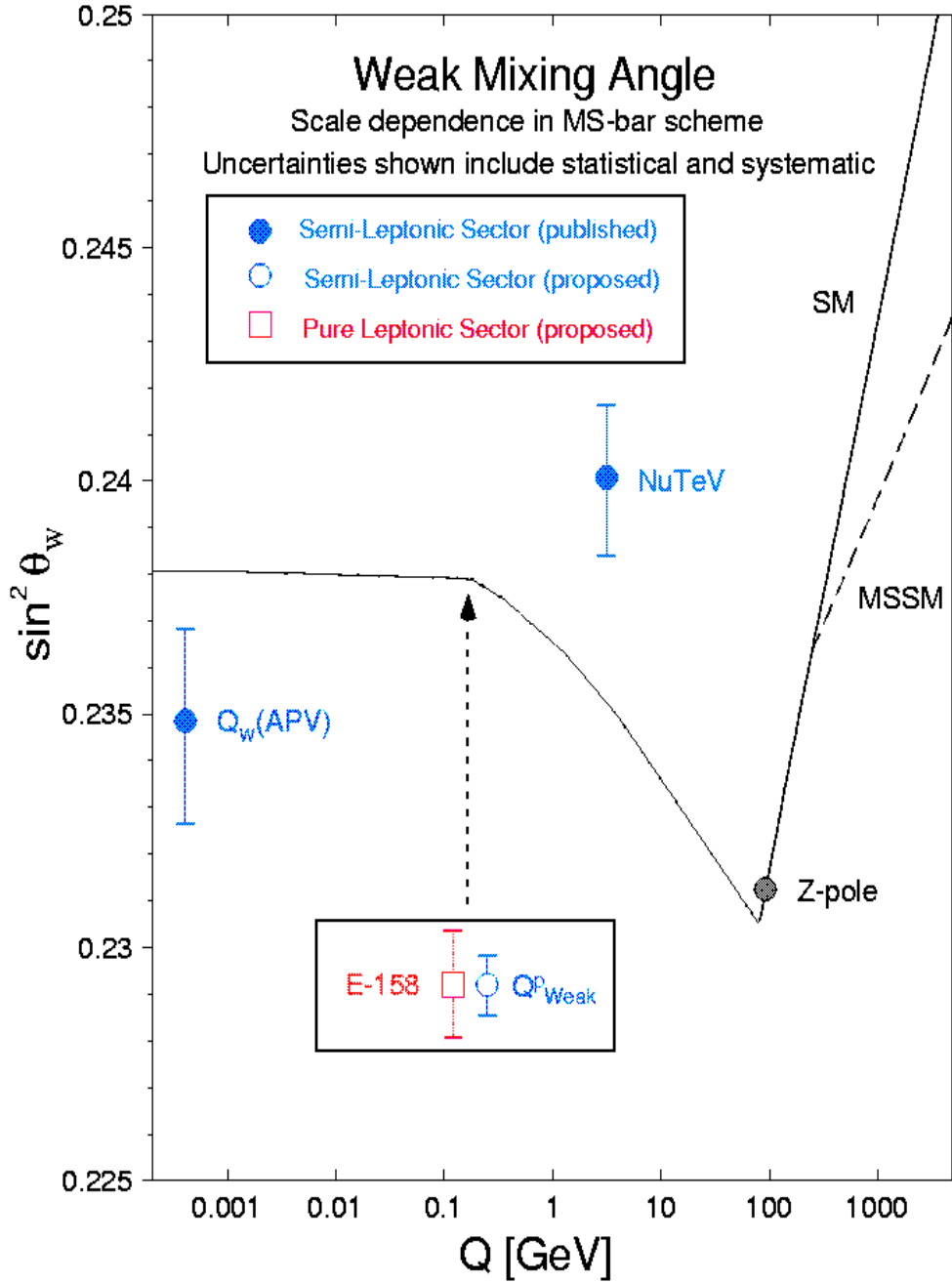


Figure 1: Calculated running of the weak mixing angle in the Standard Model, defined in the modified minimal subtraction scheme (the dashed line indicates the reduced slope typical for the Minimal SuperSymmetric Standard Model). The solid error bars show the current situation, while the open symbols (with arbitrarily chosen vertical location) refer to the asymmetry measurements proposed here and for SLAC E-158. The previous measurements are determinations from atomic parity violation (APV), deep inelastic neutrino-nucleus scattering (NuTeV), and from  $Z^0$  pole asymmetries (LEP+SLC).

In the course of two years, the value of the Cesium weak charge has gone from a  $2.3\sigma$  deviation from the SM [6], to agreement after inclusion of Breit corrections to atomic wavefunctions [7], and again to a  $2.2\sigma$  deviation upon consideration of Uehling potential effects [8]. Recently, another atomic theory calculation has appeared which claims that, after consideration of additional radiative corrections not included in earlier work, the value of the weak charge no longer differs from the SM value [9]. Apparently, achieving a definitive statement about the impact of this measurement awaits the resolution of theoretical issues which have not yet shown signs of converging to a unique solution. Nonetheless, we can combine the most precise value for the polarizability [6,10] with the most recent theory calculation [9] (quoting a more conservative error estimate) and find,  $Q_W^{Cs} = 72.24 \pm 0.28(\text{exp}) \pm 0.49(\text{th}) = 72.24 \pm 0.56$ . Combining this with  $Q_W^{Tl}$  we can extract the weak mixing angle at very low  $Q^2$ , and find a result which is  $1.6\sigma$  below the SM prediction.

Very recently, the NuTeV Collaboration [11] determined  $\sin^2 \theta_W$  at  $Q^2 \sim 10 \text{ (GeV/c)}^2$  in deep inelastic scattering of neutrinos from an approximately isoscalar (BeO) target. The result is about  $3\sigma$  above the Standard Model expectation, and has a slightly greater precision than the one from atomic parity violation. The uncertainty is claimed to be dominated by statistics. It is conceivable that isospin symmetry violating parton distribution functions are responsible for part of the effect, but it seems difficult to account for the entire deviation in this way. The deviations seen by NuTeV and in atomic parity experiments may well be due to unknown systematic or theoretical effects; on the other hand, they may also be a hint at new physics in a sector which has never been tested precisely.

Fig. 1 shows that both the measurement of  $Q_W^p$  proposed here and the polarized Møller scattering experiment E-158 [4] at SLAC, should be able to measure the weak mixing angle at low energies to unprecedented precision. These experiments will have different systematic errors and complementary dependences on physics beyond the Standard Model. A 4% measurement of  $Q_W^p$  corresponds to an uncertainty of  $\pm 0.0007$  in  $\sin^2 \theta_W$ , and would establish the *difference* in radiative corrections between  $\sin^2 \theta_W(Q^2 \approx 0)$  and  $\sin^2 \theta_W(M_Z)$  as a 10 standard deviation effect. For comparison, the E-158 Collaboration envision a combined statistical and systematic error of  $\sim 9\%$  [4,5] on the measured asymmetry.

## 2.2 Beyond the Standard Model

From a theoretical standpoint, there exist strong reasons to believe that the Standard Model is only a low energy effective theory within some larger framework. These reasons include the large number of parameters (masses, mixing angles, couplings) which must be put in by hand rather than following as natural consequences of the theory; the mass hierarchy problem; and the apparent lack of coupling unification when the couplings are run perturbatively up to the expected grand unification scale. In addition, the Standard Model does not explain the observed gauge symmetries and fermion representations or why discrete symmetries such as parity are violated; it simply incorporates these phenomenological observations in the structure of the model. One expects that a more complete theory will provide deeper explanations for these features of the Standard Model and address these conceptual open questions.

Looking beyond the Standard Model, precision measurements are beginning to sketch the

outlines of a more complete theory. In addition to the suggestive results for the running of  $\sin^2 \theta_W$  from atomic parity violation and NuTeV experiments, the azimuthal dependence of the atmospheric  $\nu_\mu$  deficit observed by the Super Kamiokande collaboration implies nearly maximal mixing between the  $\nu_\mu$  and  $\nu_\tau$ . Furthermore, the recent results for the anomalous magnetic moment of the muon [15],  $(g - 2)_\mu$ , show a  $2.5\sigma$  deviation from the Standard Model, providing tantalizing hints of supersymmetry if questions regarding hadronic loop effects can be settled. Confirmation of the  $(g - 2)_\mu$  result in other regimes is essential to determining which extensions of the Standard Model should be pursued, and therefore low energy experiments will continue to play an important role in the search for this more complete theory. Experiments at the  $Z^0$  pole are sensitive to new physics (such as modifications of the Standard Model vector boson propagators) which affect physics at  $s \simeq M_Z^2$ . Low energy electroweak observables, on the other hand, are sensitive to new physics which does not sit resonate with the  $Z^0$  boson such as a  $Z'$  boson with  $M_{Z'} \neq M_{Z^0}$ .

In the present experiment, we propose to measure the weak charge of the proton,  $Q_W^p$ . The proton's weak charge is a fundamental property of the proton which has never been measured. It is the neutral current analog of the vector coupling  $G_V$  which enters neutron and nuclear  $\beta$ -decay. In contrast to  $Q_W(Z, N)$  for a heavy atom, which is a large number of order  $N$ , the observable  $Q_W^p$  is fortuitously suppressed in the Standard Model. This is because  $Q_W^p = 1 - 4 \sin^2 \theta_W$  and the value of the weak mixing angle,  $\sin^2 \theta_W$ , is numerically close to  $1/4$ . This is characteristic for protons and electrons but *not* neutrons, making a weak charge measurement on the proton particularly sensitive to deviations arising from new physics. Consequently, the required experimental precision is about an order of magnitude less stringent than needed for atomic parity violation new physics searches. Roughly speaking, a 13% measurement of  $Q_W^p$  is equivalent in new physics sensitivity to a 1% measurement of  $Q_W(N, Z)$ . Moreover, the parity violating  $ep$  asymmetry,  $A_{LR}(^1H)$ , is sufficiently free from theoretical uncertainties at low  $Q^2$  to make it interpretable as a new physics probe.

### 2.2.1 Model independent constraints

Before considering the implications for particular models of new physics, it is instructive to consider the model independent implications of our proposed 4%  $Q_W^p$  measurement. As discussed further in Appendix B, the low-energy effective *electron – quark* Lagrangian of the form  $A(e) \times V(q)$  is given by,

$$\mathcal{L} = \mathcal{L}_{SM}^{PV} + \mathcal{L}_{NEW}^{PV}, \quad (1)$$

where

$$\mathcal{L}_{SM}^{PV} = -\frac{G_F}{\sqrt{2}} \bar{e} \gamma_\mu \gamma_5 e \sum_q C_{1q} \bar{q} \gamma^\mu q, \quad (2)$$

$$\mathcal{L}_{NEW}^{PV} = \frac{g^2}{4\Lambda^2} \bar{e} \gamma_\mu \gamma_5 e \sum_f h_V^q \bar{q} \gamma^\mu q, \quad (3)$$

where  $g$ ,  $\Lambda$ , and the  $h_V^q$  are, respectively, the coupling constant, the mass scale, and effective coefficients associated with the new physics. The Standard Model coefficients take the values

$C_{1u}/2 = -0.09435 \pm 0.00011$  and  $C_{1d}/2 = +0.17068 \pm 0.00008$  [63], for up and down quarks, respectively, and one can write

$$Q_W^p(\text{SM}) = -2(2C_{1u} + C_{1d}) \approx 0.0721. \quad (4)$$

In Fig. 2, we plot the present constraints on  $\Delta C_{1u}$  and  $\Delta C_{1d}$ , the shifts in the  $C_{1q}$  caused by new physics. The present constraints are derived from the Cesium weak charge results [6] and MIT-Bates  $^{12}\text{C}$  [16] and SLAC Deuterium parity violation measurements. As long as  $h_V^u$  and  $h_V^d$  are almost perfectly correlated, only an extremely weak limit on the mass-to-coupling ratio  $\Lambda/g$  can be derived from the data. The impact of the proposed  $Q_W^p$  measurement is indicated by the ellipse, assuming the experimental central value equals the Standard Model prediction. The dramatic reduction in the allowed phase space for new physics in this model-independent parameterization arises from the high precision of the  $Q_W^p$  measurement and its complementarity to existing data.

A 4% measurement of  $Q_W^p$  would test new physics scales up to

$$\frac{\Lambda}{g} \sim \frac{1}{\sqrt{\sqrt{2}G_F|\Delta Q_W^p|}} \approx 4.6 \text{ TeV}. \quad (5)$$

The sensitivity to non-perturbative theories (such as technicolor and other strong coupling dynamics) with  $g \sim 2\pi$  could even reach  $\Lambda \approx 29$  TeV. While limits within particular models may vary (for a recent review, see Ref. [14]), this model independent analysis illustrates the decisive role a  $Q_W^p$  measurement could play.

Turning to specific theoretical extensions of the Standard Model, of which there are many, we focus next on three particularly well-motivated cases as examples and show the impact of our proposed  $Q_W^p$  measurement. (A lengthier discussion of these cases and how the estimates were arrived at is given in Appendix B.)

### 2.2.2 Extra neutral gauge interactions

The introduction of neutral gauge symmetries beyond those associated with the photon and the  $Z$  boson have long been considered as one of the best motivated extensions of the Standard Model. In the context of supersymmetry, they do not spoil the approximate gauge coupling unification predicted by the simplest and most economic SUSY scenarios. From a phenomenological standpoint, direct searches at the Tevatron [17] have as yet yielded no firm evidence for the existence of the extra neutral  $Z'$  boson associated with the  $U(1)'$  symmetry group, providing instead only lower bounds of about 600 GeV (depending on the precise nature of the  $Z'$ ). On the other hand, both the atomic parity violation and the NuTeV determinations of  $\sin^2 \theta_W$ , which disagree with Standard Model predictions, can be brought into better agreement when one allows a  $Z'$ .

As discussed in Appendix B, the  $Z'$  can be written as a linear combination:

$$Z' \sim -\cos \alpha \cos \beta Z_\chi + \sin \alpha \cos \beta Z_Y - \sin \beta Z_\psi. \quad (6)$$

To study the impact of a  $Z'$  on  $Q_W^p$  we consider the current best fit values,  $\alpha = -0.8_{-0.8}^{+1.2}$ ,  $\beta = 1.2_{-0.4}^{+0.2}$ , and the  $Z^0 - Z'$  mixing parameter  $\sin \theta = 0.0009_{-0.0006}^{+0.0007}$ . In this case,  $Q_W^p$

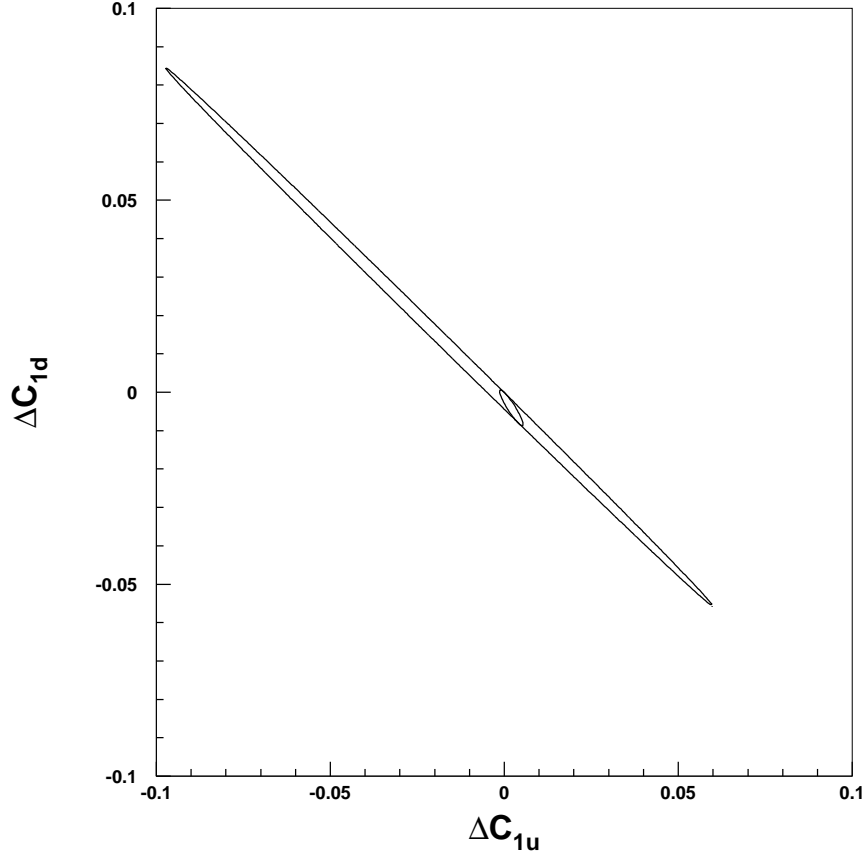


Figure 2: Present and prospective 90% C.L. constraints on new physics contributions to *electron – quark* couplings,  $\Delta C_{1a}$ . The larger ellipse denotes the present limits, derived from Cesium APV, the MIT-Bates PV electron scattering measurement from  $^{12}\text{C}$ , and the SLAC PV electron scattering measurement from Deuterium. The smaller ellipse indicates the constraints after the inclusion of the  $Q_W^p$  measurement, assuming the central experimental value coincides with the Standard Model prediction. The reduction in allowed phase space is dramatic.

$= 0.0780$  is predicted, which is a  $+2\sigma$  effect. If the physical value of  $Q_W^{Cs}$  is at the lower end of its  $1\sigma$  allowed range, the best prediction would be  $Q_W^p = 0.0810$ , which is  $+3.1\sigma$  above the Standard Model expectation.

Thus, one of the most straightforward and best motivated extensions of the Standard Model describes the current data better than the Standard Model itself and predicts a significant deviation in  $Q_W^p$ . In view of the very high precision and very high energy measurements at the  $Z^0$  factories LEP and SLC, it is quite remarkable that a 4% measurement at very low  $Q^2$  and operating with a several orders of magnitude lower budget offers a more sensitive probe of TeV scale physics. If the SLAC E-158 and  $Q_W^p$  measurements show results consistent with a  $Z'$  and with each other, they could be combined, offering strong evidence for the new force.

Even if a  $Z'$  were detected at the Tevatron or the LHC first, it would be important to constrain its properties. Its mass will be measured in course of the discovery, and the  $Z - Z'$  mixing parameter  $\sin\theta$  is mainly constrained by LEP 1. The  $U(1)'$  charges and the couplings to quarks and leptons, however, are best determined by low-energy precision measurements. The allowed regions of the parameters  $\alpha$  and  $\beta$  of the case above can be decreased by 40%. For example, if  $Q_W^p$  is found to be  $3\sigma$  above the Standard Model prediction, the parameter  $\alpha$  would be significantly different from zero, while a  $4\sigma$  effect would establish the mixing with hypercharge with more than 90% confidence.

### 2.2.3 Other models: supersymmetry and leptoquarks

Supersymmetry (SUSY) has long been considered a likely ingredient of an “extended” Standard Model. The theoretical motivation includes superstring theories, for which the existence of SUSY is a prediction; resolution of the “hierarchy problem” associated with Higgs mass renormalization and stability of the weak scale without resorting to fine tuning of parameters; and gauge coupling unification at the GUT scale. From a phenomenological standpoint, the recently reported deviation of the muon anomaly from the Standard Model prediction provides a tantalizing hint of SUSY, since contributions from “superpartner” loops provide a natural explanation for the effect.

In Appendix B, we discuss the present SUSY constraints relevant to charged and neutral current interactions of light quarks and leptons in detail. The present world data could accommodate a  $+9\%$  ( $+10\%$ ) shift in  $Q_W^p$  at 90% (95%) C.L. Depending on the outcome of the proposed  $Q_W^p$  measurement, the impact on this new physics could be severe. At present, SUSY provides one of the only simultaneous explanations of both the charged current and neutral current low-energy deviations from the Standard Model (superallowed  $\beta$ -decay and Cesium atomic PV, respectively). The  $Q_W^p$  measurement would provide an important diagnostic as to whether this solution remains a viable one. In contrast, the prospective impact of the parity violating Møller asymmetry measurement (SLAC E-158) is less pronounced, since it competes directly with  $W$ -mass measurements. A comparison of  $Q_W^p$  and Møller results, however, could provide additional information. For example, were both measurements to agree with each other, while disagreeing with the SM, it would be less likely that R-parity violating SUSY interactions were responsible for the effect.

We turn next to leptoquarks – bosons which have both nonzero baryon and lepton number,

which have long been a popular, though somewhat exotic, candidate for new physics. The implications of electroweak data for scalar leptoquark models have been analyzed most recently in Refs. [18,19]. In the analysis of Ref. [18] (at which point the Cesium atomic parity violation results were interpreted to show a  $2.3\sigma$  deviation from the Standard Model), two species of leptoquarks were found to provide an explanation for the effect while maintaining consistency with all other electroweak data. The presence of these leptoquarks would also induce a shift in  $Q_W^p$  – an effect of up to  $3\sigma$  in our proposed experiment is not ruled out by existing data. It should be noted that the same leptoquarks could also produce significant deviations of  $Q_W^p$  from the Standard Model prediction even if the Cesium weak charge result is taken to agree with the Standard Model (see Appendix B for discussion).

We note that, as in the case of other scenarios discussed above, the comparison of a  $Q_W^p$  measurement with results of the Møller parity violation experiment provides a powerful diagnostic. Leptoquark effects enter parity violating Møller scattering only at loop level, and their effects are considerably smaller than the anticipated precision of the E-158 measurement [14]. Thus, should both experiments deviate from the Standard Model prediction by two or more standard deviations, one would suspect the effect was *not* generated by leptoquarks.

#### 2.2.4 Summary

We have demonstrated that the proposed measurement of  $Q_W^p$  at Jefferson Laboratory will provide a stringent test of the Standard Model prediction for the running of  $\sin^2 \theta_W$ . In the case of agreement with the Standard Model, our measurement will provide the single most significant confirmation of this essential prediction of the running coupling constant away from the  $Z^0$  pole, and the result will dramatically reduce the model-independent phase space for possible new parity violating electron-quark couplings. In *any* case, our experiment will provide important new constraints on new physics. We have explored the implications of existing world data for possible deviations that might be seen in our  $Q_W^p$  experiment in the context of several strong candidate extension theories, and we conclude that the proposed measurement can have a high impact. This is illustrated, together with the anticipated errors from SLAC E-158, in Figure 3. The two experiments will have a similar sensitivity to extra  $Z'$  bosons, but different sensitivities to R-parity violating SUSY and leptoquark based models.

### 2.3 Theoretical Interpretability

A particularly attractive feature of the proposed  $Q_W^p$  measurement is the unambiguous character of its theoretical interpretation. The recent variations in atomic theory calculations for Cesium atomic parity violation underline the importance of this consideration. Use of a proton target offers the simplest possible system on which to perform a low-energy search for new neutral current physics in the semileptonic sector. As in the case of neutron  $\beta$ -decay, where a combination of measurements (lifetime and asymmetry parameter) allow one to perform an extraction of the charged current vector coupling constant with minimal hadronic complications, the proposed measurement of  $Q_W^p$  – in conjunction with the anticipated results of the G0, HAPPEX, SAMPLE, and Mainz parity-violation experiments – will allow for a clean determination of the

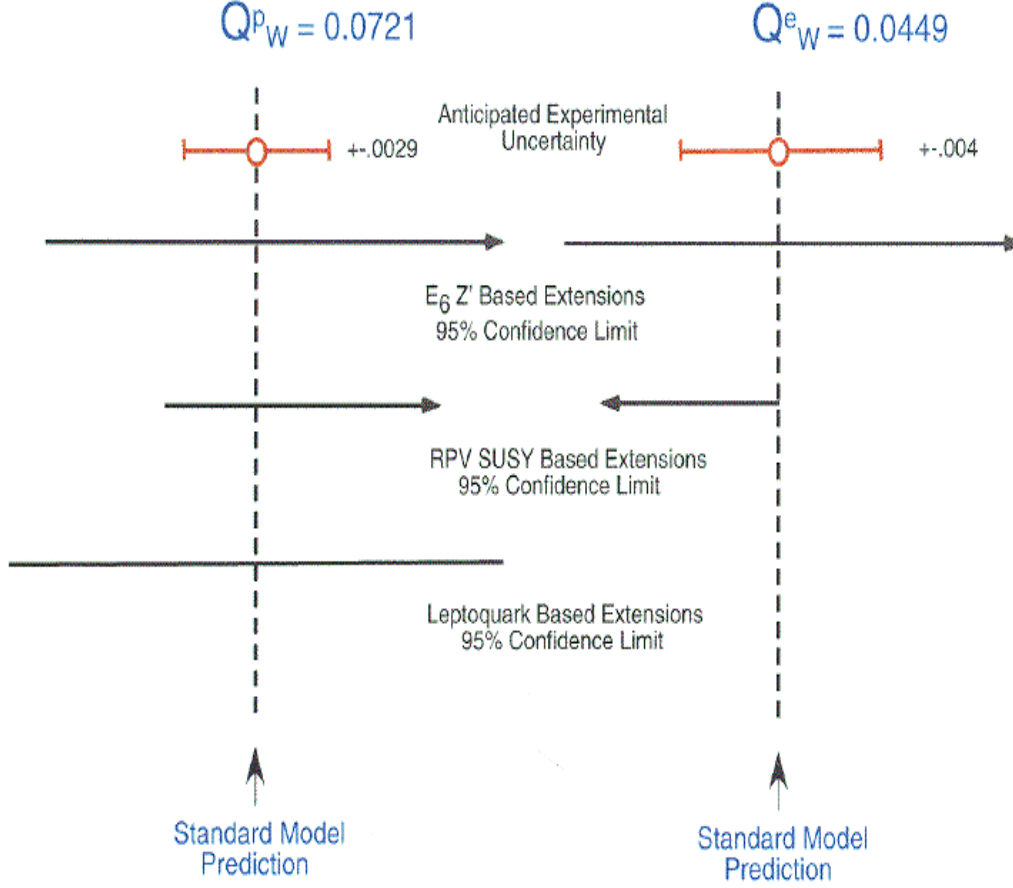


Figure 3: Comparison of expected errors for  $Q_W^p$  and  $Q_W^e$  with possible deviations from the Standard Model allowed by fits to existing world data in the context of several plausible extension theories. Note that the two measurements are highly complementary. With respect to their sensitivity and sign, both measurements will shift significantly due to a  $Z'$  and thus together they could result in strong evidence for such new physics. In the case of SUSY based extensions, the two measurements are somewhat anti-correlated with respect to the change produced on the measured weak charge. Finally, in the case of leptoquarks, only the  $Q_W^p$  measurement will be sensitive while the  $Q_W^e$  measurement serves as a control. Together, these measurements have the potential to produce strong evidence for physics beyond the Standard Model and possibly even a signature with respect to the nature of the physics.

weak neutral current vector coupling constant (*i.e.*,  $Q_W^p$ ). Once  $Q_W^p$  is determined, the extraction of information on various new physics scenarios is similarly free from theoretically uncertain corrections, as alluded to above.

The quantity  $A_{LR}(^1H)$  (henceforth simply  $A$ ) is the asymmetry in the measurement of the cross section difference between elastic scattering by longitudinally polarized electrons with positive and negative helicities from unpolarized protons:

$$A = \frac{\sigma_+ - \sigma_-}{\sigma_+ + \sigma_-}, \quad (7)$$

which, expressed in terms of Sachs electromagnetic form factors  $G_E^\gamma, G_M^\gamma$ , weak neutral form factors  $G_E^Z, G_M^Z$  and the neutral weak axial form factor  $G_A$ , has the form [20]:

$$A = \left[ \frac{-G_F Q^2}{4\pi\alpha\sqrt{2}} \right] \left[ \frac{\varepsilon G_E^\gamma G_E^Z + \tau G_M^\gamma G_M^Z - (1 - 4\sin^2\theta_W)\varepsilon' G_M^\gamma G_A^Z}{\varepsilon(G_E^\gamma)^2 + \tau(G_M^\gamma)^2} \right] \quad (8)$$

where

$$\varepsilon = \frac{1}{1 + 2(1 + \tau)\tan^2\frac{\theta}{2}}, \quad \varepsilon' = \sqrt{\tau(1 + \tau)(1 - \varepsilon^2)} \quad (9)$$

are kinematical quantities,  $Q^2$  is the four-momentum transfer,  $\tau = Q^2/4M^2$  where  $M$  is the proton mass, and  $\theta$  is the laboratory electron scattering angle. It was shown in [21] that for forward-angle scattering where  $\theta \rightarrow 0$ ,  $\varepsilon \rightarrow 1$ , and  $\tau \ll 1$ , the asymmetry can be written as:

$$A = \left[ \frac{-G_F}{4\pi\alpha\sqrt{2}} \right] \left[ Q^2 Q_w^p + F^p(Q^2, \theta) \right] \rightarrow \left[ \frac{-G_F}{4\pi\alpha\sqrt{2}} \right] \left[ Q^2 Q_w^p + Q^4 B(Q^2) \right] \quad (10)$$

where  $F^p$  is a form factor. Neglecting radiative corrections, the leading term in the equation is simply  $Q_w^p = 1 - 4\sin^2\theta_W$ . The  $B(Q^2)$  is the leading term in the nucleon structure defined in terms of neutron and proton electromagnetic and weak form factors. An accurate measurement of  $\sin^2\theta_W$  thus requires higher order, yet significant, corrections for nucleon structure. Nucleon structure contributions in  $B(Q^2)$  (which enter to order  $Q^4$ ) can be reduced by going to lower momentum transfer. However, this also reduces the sensitivity to  $Q_w^p$  (which enters to leading order in  $Q^2$ ) making it statistically more difficult to measure. The value of  $B(Q^2)$  can be determined experimentally by extrapolation from the ongoing program of forward angle parity-violating experiments at higher  $Q^2$ . We have estimated the optimum value of  $Q^2$  to be near  $0.03 (GeV/c)^2$  based on our estimate of the anticipated precision of the various HAPPEX,  $G^0$ , and Mainz A4 measurements. As shown in Section 3.7.3, we anticipate the error on  $Q_w^p$  from nucleon structure contributions to be about 2%.

The remaining theoretical uncertainties are those which enter  $Q_w^p$  itself. Strong interaction uncertainties entering the Standard Model prediction for  $Q_w^p$  lie below the proposed experimental error. The sources of these uncertainties include the following:

- (i) Hadronic contributions to the running of  $\sin^2\theta_W$ :  $\Delta Q_w^p \sim \pm 0.4\%$
- (ii) Strong corrections to  $\gamma Z$ -box graphs:  $\Delta Q_w^p \sim \pm 0.6\%$

- (iii) Strong corrections to  $WW$ -box graphs:  $\Delta Q_W^p \sim \pm 1.5\%$
- (iv) Strong corrections to  $ZZ$ -box graphs:  $\Delta Q_W^p \sim \pm 0.15\%$
- (v) Isospin-breaking effects in nucleon current matrix elements, second order in isospin breaking hadronic interaction:  $\Delta Q_W^p \sim \pm \text{few} \times 10^{-5}$

Finally, there is the uncertainty in  $\sin^2 \theta_W$  determined from experiments at the  $Z$ -pole. This contributes an uncertainty of  $\Delta Q_W^p \sim \pm 0.8\%$ .

In conclusion, the theoretical errors in  $Q_W^p$  are small compared to our anticipated total uncertainty of  $\pm 4.0\%$ .

### 3 The Experiment

The overall layout of the experiment is shown schematically in Figure 4. To achieve the required statistical precision in an acceptable amount of running time, we propose to use a toroidal magnet to measure electrons scattered to small angles. Between the scattering chamber and the magnet coils, the electrons will pass through channels filled with Helium gas at atmospheric pressure. Accurately machined and aligned collimators will define the  $Q^2$  acceptance. The electrons will be detected in quartz Cerenkov detectors, converted to current signals using phototubes, and the signals will be integrated. A new high power cryotarget will be used. A 2200 hour measurement employing  $180 \mu A$  of 80% polarized beam on a 35 cm liquid Hydrogen target will be used to determine the proton's weak charge to  $\simeq 4\%$  combined statistical and systematic uncertainty. This and other basic parameters of the experiment are presented in Table 1.

#### 3.1 Spectrometer Magnet

A new resistive toroidal magnet is our preferred choice because of the low cost and the inherent reliability relative to a superconducting solution. The  $Q_{weak}$  Toroidal Magnet (QTOR) will be somewhat similar to the BLAST magnet. [22] Construction of a new, resistive magnet would allow us to execute the  $Q_{weak}$  experiment in a timely and potentially hall-independent manner: the experiment could take beam for its first engineering run 4 years after approval. Recycling a toroidal magnet built originally for a different experiment (eg, the  $G^0$  magnet), could not even begin until the end of that experimental program. However, we have done simulations for both our preferred resistive option and for the  $G^0$  magnet to show that more than one viable option exists. The resistive option is presented here; the  $G^0$  magnet option is found in Appendix A.

The  $Q_{weak}$  experiment requires detection of electrons with a forward scattering angle of  $\theta_e = 9 \pm 2$  deg. To allow for this, 8 racetrack coils are connected to a cylindrical hub, concentric to the beam axis, to form a toroidal magnet. (See Figure 5.) It is not an enormous device, fitting in a cube of dimensions 3.3m x 3.3m x 4.5m, or slightly larger than a typical CEBAF Center office. The inner radius of the hub will be 15 cm. The target position is located 750 cm upstream from the midpoint of the magnet.

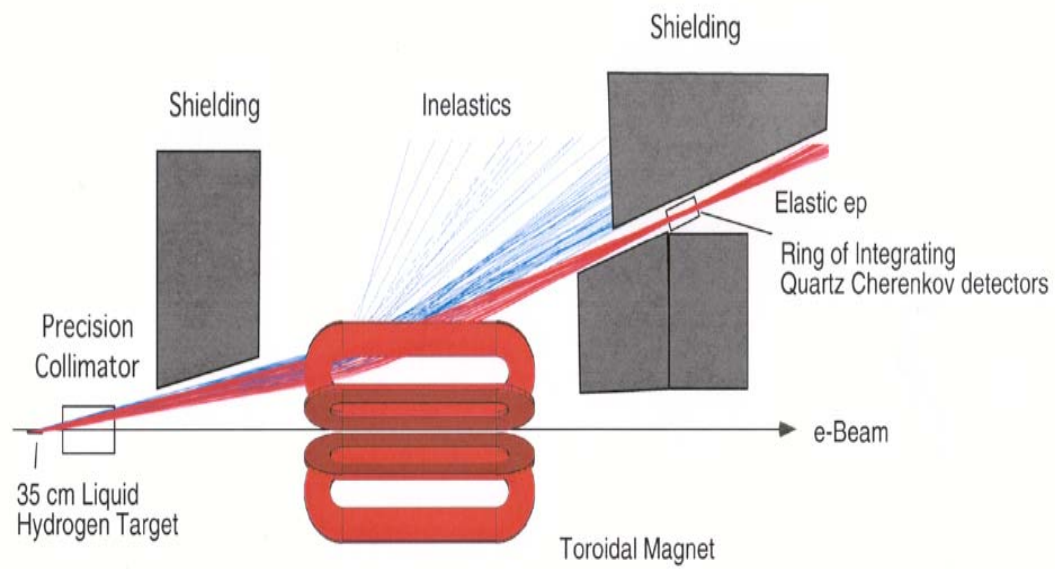


Figure 4: Artist's conception of the experiment showing the target, collimation, shielding, electron trajectories, and detectors. Elastically scattered electrons (red tracks) focus on the detectors while inelastically scattered electrons (blue tracks), are swept away from the detectors.

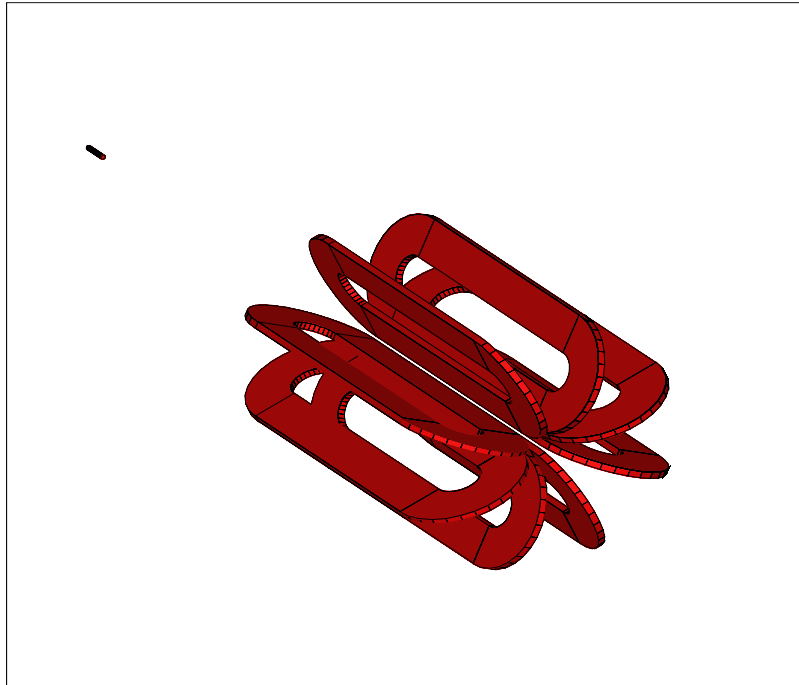


Figure 5: The shapes and the positions of the  $Q_{weak}$  Toroidal Magnet coils relative to the beam line and the position of the target.

Table 1: Basic parameters of the  $Q_{weak}^p$  experiment. The cross section and rate includes corrections for internal and external Bremsstrahlung. The statistical error on the asymmetry includes a small contribution due to finite detector noise ( 12% resolution assumed).

<u>Parameter</u>	<u>Value</u>
Incident Beam Energy	1.165 GeV
Beam Polarization	80%
Beam Current	180 $\mu$ A
Target Thickness	35 cm (0.04 $X_0$ )
Running Time	2200 hours
Nominal Scattering Angle	9°
Scattering Angle Acceptance	$\pm 2^\circ$
$\phi$ Acceptance	66.7% of $2\pi$
Solid Angle	$\Delta\Omega = 45.7$ msr
Acceptance Averaged $Q^2$	$\langle Q^2 \rangle = 0.030$ (GeV/c) <sup>2</sup>
Acceptance Averaged Physics Asymmetry	$\langle A \rangle = -0.28$ ppm
Acceptance Averaged Expt'l Asymmetry	$\langle A \rangle = -0.23$ ppm
Integrated Cross Section	3.7 $\mu$ b
Integrated Rate (all sectors)	6.1 GHz (or 763 MHz per sector)
Statistical Error on the Asymmetry	2.0%
Statistical Error on $Q_W^p$	2.8%

### 3.1.1 Resistive coil geometry and cost estimate

Each coil will have a race-track shape, with two 300 cm long straight sectors and two semi-circular sectors with inner radius 25 cm and outer radius 75 cm. (The coil cross section will be rectangular, 8 cm thick by 50 cm wide.) Some requirements imposed on the BLAST magnetic field, such as the field free region for internal polarized targets, are not relevant for the  $Q_{weak}$  measurement. Therefore, the  $Q_{weak}$  coils will have a simpler shape and should cost less. The total length of the QTOR will be 450 cm, slightly longer than the 434 cm length of the BLAST magnet.

### 3.1.2 Magnetic field calculations and optics

To a large extent, the magnet design is driven by the field integral required to bend  $\theta_e = 9.0$  deg scattered electrons with momentum  $P' \simeq 1.150$  GeV/c by approximately  $\Delta\theta_e = 10.0$  deg. (A larger bending angle provides greater dispersion, but one also needs to keep the azimuthally-symmetric detector package from running into the floor.) The required field integral is approximately 0.67 T·m, which is about half the  $G^0$  magnet  $\int Bdl = 1.6$  T·m [23] It is comparable to the normal-conducting toroidal magnet BLAST where the field integral is between 0.2 and 0.6 T·m [22]. Thus, a superconducting solution is not required. In fact, our preferred resistive solution looks like a simplified, but slightly larger, version of the BLAST magnet.

The GEANT simulation software package [25,26] was used for the design of the experimental setup. Two software packages were written to calculate the magnetic field and to design the

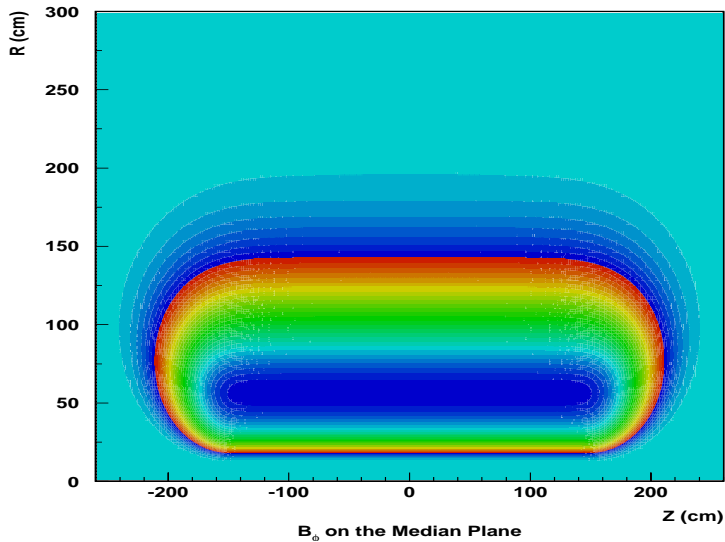


Figure 6: Contour plot of the azimuthal magnetic field components  $B_\phi$  on the median plane between two coils. Step sizes are 0.2 KGauss.

$Q_{weak}$  magnet. Only a small portion of the magnetic optics studies are presented in this proposal. Complete details can be found in the report by Simicevic. [27]

The magnetic field was calculated using the Biot-Savart Law and a finite element treatment of the current density. A coil was represented by arcs and straight conductor segments. The magnetic field for the  $Q_{weak}$  magnet was calculated assuming a current density of 505 A/cm<sup>2</sup>. This current density is roughly consistent with the nominal design rule-of-thumb of a maximum current density of 500 A/cm<sup>2</sup> for insulated, water-cooled copper windings. If needed, higher current densities are possible. With proper choice of insulation and adequate (but not erosive) water flow, current densities as high as 600 A/cm<sup>2</sup> should not be a major problem. [28]

A contour plot of the azimuthal magnetic field components,  $B_\phi$ , is shown in Figure 6. The shape of the coil is reflected in the contours. The field on the beam axis is zero, and increases rapidly, reaching a maximum of 0.33 T at a distance of 56 cm from the beam axis. From that point, the field falls off as 1/R. Since the target is outside and upstream of the magnet, the field integral seen by an electron depends on the scattering angle. Because electrons with smaller polar angle  $\theta_e$  have more  $\int Bdl$  than the electrons at larger polar angles, the result is focusing of the elastically scattered electrons.

Four profiles of the azimuthal magnetic field component  $B_\phi$  as a function of radial distance R are shown in Figure 7. The field component  $B_\phi$  is calculated in the median plane and the plane corresponding to the limiting azimuthal angle of  $\phi = \pm 15$  deg from the median plane for two positions along the beam axis: the center of the magnet at  $z = 0$ , and close to the ends of the magnet at  $z = \pm 200$  cm. Field uniformity versus  $\phi$  is adequate.

Scattered electron trajectories are shown in Figure 8. It is clear that for elastic scattering, the magnet indeed has the required focusing behavior. A similar plot of trajectories can be made

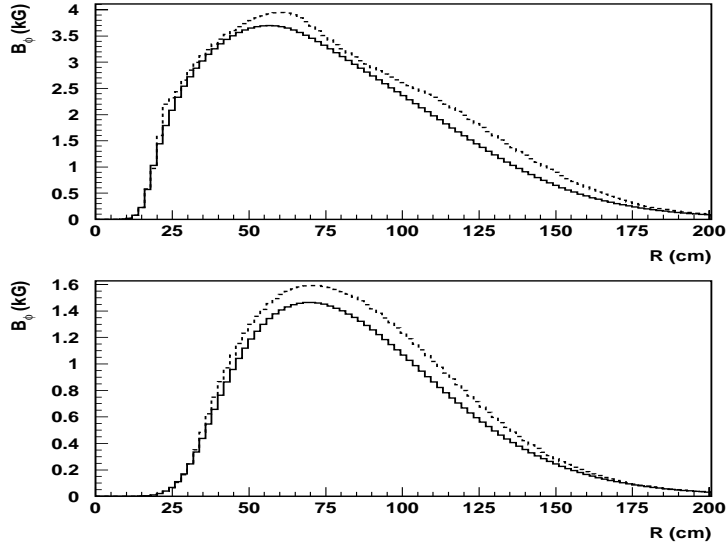


Figure 7: The azimuthal magnetic field components  $B_\phi$  on the median plane between two coils (full line) and at the plane corresponding to the limiting azimuthal angle of  $\phi = \pm 15$  deg (dashed line). The top histogram is for  $z = 0$  cm, corresponding to the center of the magnet, and the bottom for  $z = \pm 200$  cm, close to ends of the magnet.

for the  $G^0$  magnet and is found in Appendix A.

Regarding the effects of misalignment, while these have not yet been studied in detail for the  $Q_{weak}$  magnet, similar studies for the  $G^0$  superconducting magnet showed that the tolerances were easily achieved.

The BLAST toroid and power supply cost roughly \$700K. The QTOR proposed here is slightly larger, but has a much simpler coil design. We assume the QTOR and power supply cost will be \$600K, pending a detailed design. Assuming the  $G^0$  magnet were available in time, the cost for recycling it would have to be determined by an engineering review.

## 3.2 Detection

### 3.2.1 Rate estimate

To help define the type of detector, we have to first estimate the counting rates using the information in Table 1. Counting rates for the elastically scattered electrons are then calculated using the formula

$$Rates = L \times \int_{\Delta\Omega} \frac{d\sigma}{d\Omega} d\Omega, \quad (11)$$

where  $L$  is the luminosity, and  $\frac{d\sigma}{d\Omega}$  is the elastically scattered electron differential cross section, with the electromagnetic form factors in a dipole parameterization. The luminosity was calculated to be  $1.76 \times 10^{39} \text{ cm}^{-2}\text{s}^{-1}$ . The integrated, radiated cross section from Table 1 is  $3.7 \mu\text{b}$  leading

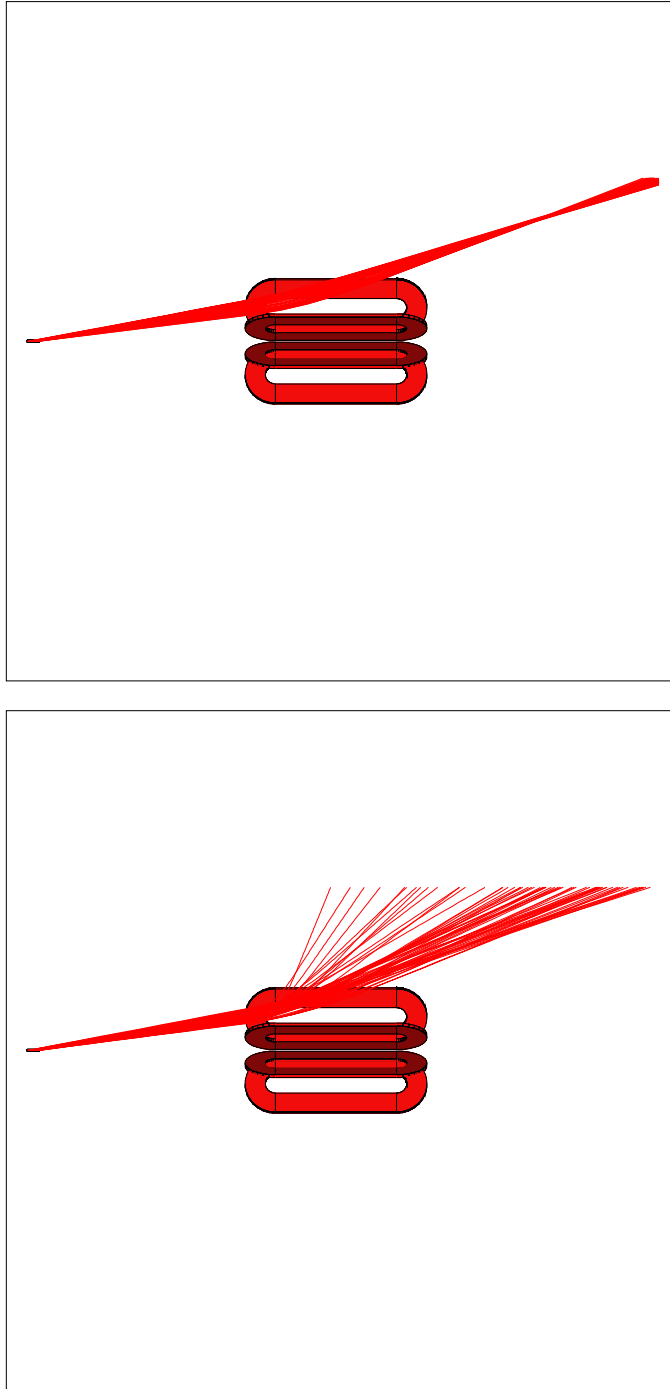


Figure 8: The side view of the test setup with a sample of elastic (top) and inelastic (bottom) trajectories collimated to  $\theta_e = 9 \pm 2$  deg and  $\phi_e = 0.0 \pm 15$  deg. The correlation between scattering angle and field integral produces a focus for elastic trajectories.

to a total rate of 6.1 GHz or 763 MHz per detector. Such high rate requires integration of the detector signals.

### 3.2.2 Detectors

Several factors drive the design of the detectors:

- This precision measurement requires high statistics; therefore, the rate should be as high as technically achievable. Radiation hardness will be an issue.
- The detector system must clearly separate the elastic and inelastic channels, and must accept nearly all the elastic events.
- Sensitivity to backgrounds (*e.g.*, low energy gammas and neutrons) should be minimized.
- Noise produced by the detector (*e.g.*, a limited number of photoelectrons) must not significantly deteriorate the ability of the experiment to achieve counting statistics.
- Reduced size and weight are helpful for reducing backgrounds and cost, and for simplifying the mounting scheme.

Quartz Cerenkov detectors will meet most of the above requirements. The use of a Cerenkov detector minimizes the sensitivity to low-energy hadrons, and quartz is very insensitive to radiation damage. The detectors consist of one rectangular quartz bar per octant. Each detector bar will be rotated slightly to be normal to the elastic electron trajectories. They will be read out on both ends by 5 inch photomultiplier tubes with S20 photocathodes.<sup>2</sup> The choice of thickness is somewhat arbitrary, but for now we have selected 1.72 cm which allows us to benefit from BaBar experience with fused silica radiator bars in their detector. [30] Specifying a modest surface reflectivity of 0.997% will provide a total of about 90 photoelectrons per traversing electron when the two ends are summed. [29] The additional statistical error on the asymmetry measurement per helicity reversal due to detector photoelectron statistics is less than 1%, ie,  $\sqrt{1 + (\sigma_{pe}/N_{pe})^2} < 1.01$ .

Figure 9 shows the elastic and inelastic tracks as they cross the detection plane. There is a clear separation between elastic and inelastic events. (Electron radiation has not yet been enabled in these simulations.) A detector with dimensions of roughly 200 cm long by 12 cm wide is adequate for containing the elastic envelope with minimal contamination from inelastic near-threshold events.

Placing several cm of lead preradiator in front of the quartz bars has the potential to increase the already large signal without adding unduly large statistical noise due to shower fluctuations. Possible advantages of this would be to further reduce the sensitivity to low energy background and to energetic  $\pi^-$ 's produced in the target windows.

---

<sup>2</sup>The relatively low sheet resistance of the S20 photocathode is important for maintaining a constant voltage over the photocathode when large photocathode currents are drawn.

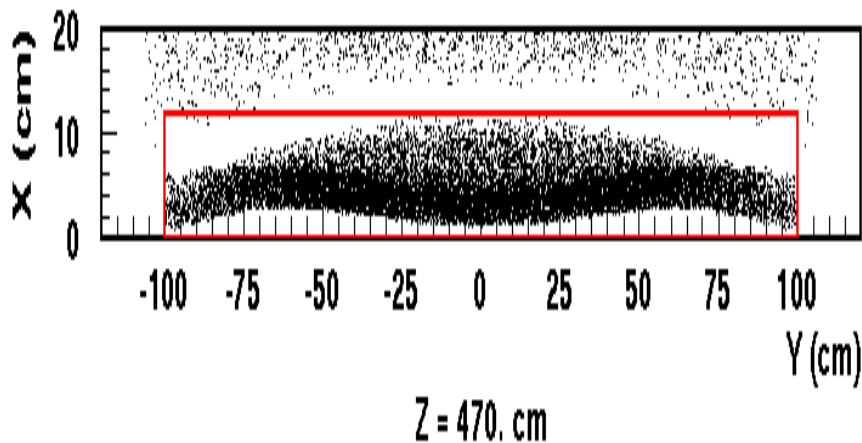


Figure 9: Separation of elastically (lower distribution) and inelastically (upper distribution) scattered electrons at the detector plane, located 425 cm downstream from the center of the magnet. The electrons are collimated to  $\theta_e = 9.0 \pm 2$  deg and  $\phi_e = 0.0 \pm 15$  deg. A preliminary detector shape, pending further simulations, has been outlined.

### 3.2.3 Electronics

Due to the high event rates associated with the  $Q_{weak}$  experiment, precision integrating techniques for parity experiments must be employed during production running. Traditional counting methods will be used during acceptance and efficiency calibration measurements. The signal processing electronics have been designed to meet the following requirements:

- The detectors must operate in both current mode and pulse mode.
- All components in the current mode configuration must be extremely linear.
- The least-count noise from the V to F converter must be small compared to counting statistics.
- The detector-preamp-converter system should be immune to ground loop pick up of the reversal signal.
- In current mode, the electronic noise must be very small compared to the counting statistics on the rate of detected electrons.

The configuration shown in Figure 10 meets all the above requirements. The two signals from each of the 8 sectors will be summed, input to a high gain ultra-linear operational amplifier I-to-V (current to voltage converter) located close to the detectors, passed to the counting house

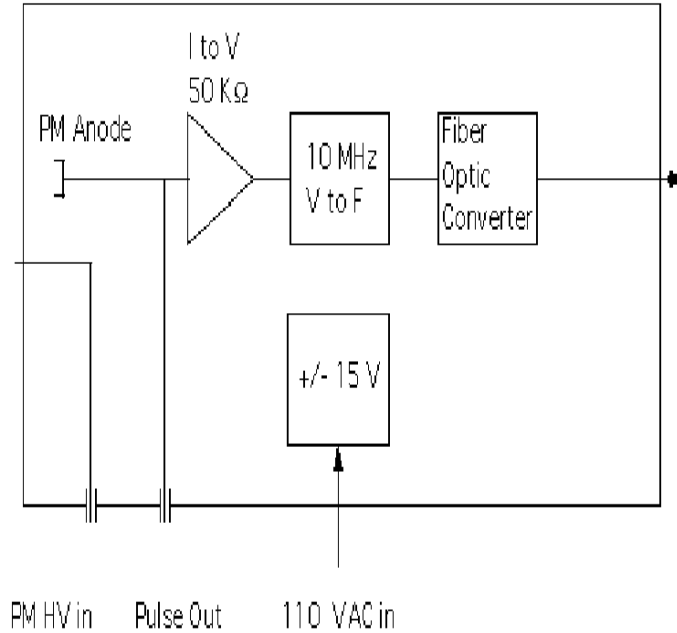


Figure 10: Conceptual design for the electronics.

by opto-isolated transmitters, fed into a linear 10 MHz V/F (Voltage-to-Frequency) converter, and finally digitized by gated scalers. The proposed helicity reversal rate would be 30 Hz with an experiment read out rate of 120 Hz. The 120 Hz readout rate is to allow for a 4 times over-sampling rejection of non-linear induced systematics from 60 Hz line couplings and prevent leakage of the reversal signal into the apparatus. The electronics are neither new nor complex, but are straightforward and have been used successfully on parity experiments at LANL and TRIUMF where small asymmetries ( $\simeq 10^{-8}$ ) were measured.

We expect a rate of 0.8 GHz/detector from electrons which gives a photo cathode current of approximately 0.7 nA. An S20 photo cathode will be used in order not to have voltage drop across the photocathode at this current. In the current mode configuration, the photo multiplier will be operated at a gain of  $5 \times 10^5$  which will give a two tube combined anode current of  $3 \times 10^{-4}$  A.

The current noise from counting statistics at the two tube anode sum is:  $I_{count} = 10^{-9} \text{ A}/\sqrt{(\text{Hz})}$ . The current noise and voltage noise of an inexpensive operational amplifier are typically  $10^{-12} \text{ A}/\sqrt{(\text{Hz})}$  and  $3 \times 10^{-9} \text{ V}/\sqrt{(\text{Hz})}$ . With a transimpedance gain of  $0.5 \times 10^5 \Omega$  the I to V amplifier would produce an output voltage of 6 Volts and the V to F converter would produce an output frequency of 6 MHz. The Johnson noise of the I to V amplifier would be  $5.6 \times 10^{-13} \text{ A}/\sqrt{(\text{Hz})}$ . The current, voltage, and Johnson noise are all small (quadratic sum,  $I_{amp} = 1.0 \times 10^{-12} \text{ A}/\sqrt{(\text{Hz})}$ ) compared to the noise from counting statistics,  $I_{count} = 9.1 \times 10^{-9} \text{ A}/\sqrt{(\text{Hz})}$ .

There are two reasons to require  $I_{amp} \ll I_{count}$ . If  $I_{amp}$  is comparable to  $I_{count}$ , then the time required to reach a given statistical error in the asymmetry is increased. Also, it is desirable to perform beam-off runs to search for false asymmetries. The time required to reach a limit on false asymmetries that is the same as the error in the physics asymmetry is  $[I_{amp}/I_{count}]^2 = 10^{-8}$ . With the present design, we can check for false asymmetries in a few minutes.

The overall linearity of the above system will be limited by the least linear component. We estimate better than  $10^{-4}$  for both the photomultiplier and the V to F converter. We expect the system to be immune to ground loop coupling of the reversal signal because in current mode the only ground connection is through the shield of the high-voltage cable. The signal is transmitted as a pulse train over a fiber-optic link. The  $\pm 15\text{V}$  power supply is isolated from the 60 Hz line by a transformer. The least count noise in one 1/30 sec. reversal period is  $2 \times 10^{-5}$ . The error from counting statistics is  $2.7 \times 10^{-4}$ . Therefore, the system satisfies the requirement that the least count noise is small compared to counting statistics.

To operate the detector in diagnostics/calibration pulse mode, we will place a signal cable and  $50 \Omega$  resistor on the pulse out connector shown on Figure 10. The  $50 \Omega$  resistor will back terminate the signal cable. The photomultiplier voltage will be increased until the gain is  $6 \times 10^6$  and the  $50 \mu\text{s}$  wide output pulse is  $\sim 100 \text{ mV}$  into  $50 \Omega$ .

### 3.3 Cryotarget

The design of the  $Q_{weak}$  experiment  $LH_2$  target is based on the following parameters: safe and reliable operation for sustained periods of time with a beam current =  $180 \mu\text{A}$ , length =  $35 \text{ cm}$  (a 4% radiation length), location  $4.75 \text{ m}$  upstream of the magnet, raster size  $\sim 2 \times 2 \text{ mm}^2$ ,  $9^\circ \pm 2^\circ$  acceptance for scattered electrons, thin windows, azimuthal symmetry, no local boiling, and minimal density fluctuations.

#### 3.3.1 Refrigeration

It is important to note that our beam current and target length requirements for a 2200 hour experiment lead to a cryogenic heat load of  $2.1 \text{ kW}$ , considerably above the present  $1.2 \text{ kW}$  capacity of the JLab End Station Refrigerator (ESR). (Commissioning of the experiment could of course be done at lower power.) This target is therefore predicated on executing one of several means to increase target cooling capacity in the endstations:

- Utilize excess CHL capacity at 4K by employing a heat-exchanger near the target and returning the warm gas directly to the CHL. (This is our preferred option.)
- Carry out the planned expansion of the ESR to twice its present capability.
- Run the existing standby refrigerator located next to the CHL. The additional cost for the electrical power would be on the order of  $\$90\text{k}$  per month.

Because the  $Q_{weak}$  collaboration will require several years to fund, prototype, and build our apparatus, we will be able to make good use of any enhanced cryogenic capacity available after the completion of SNS cavity testing.

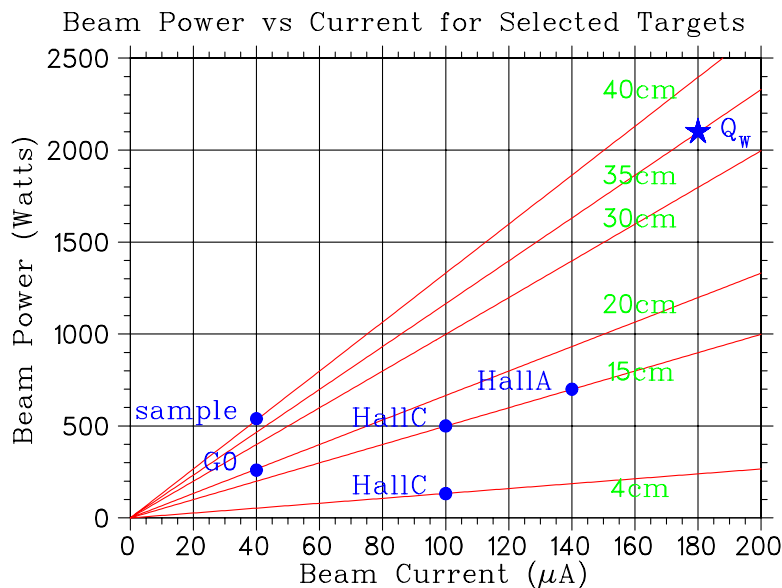


Figure 11: Values of the beam power deposited in  $LH_2$  targets as a function of beam current, for target cells varying between 4 cm and 40 cm in length. The solid point indicates the expected  $Q_{weak}$  configuration (35 cm target, 180  $\mu A$ , 2.1 kW).

To put our target coolant requirements in perspective, we show in Figure 11 a plot of beam current versus target heat load for representative  $LH_2$  targets. We note that the beam current required for  $Q_{weak}$  is only 30% higher than has already been employed in Hall A during physics production, and that the SAMPLE target at MIT Bates is only 5 cm longer than the  $Q_{weak}$  target. However, the combination of high beam current and a long target flask will make the  $Q_{weak}$  target the highest power cryotarget in the world by a factor of several. Although the experiment could be run with a lower power cryotarget, the length of the run would have to be increased correspondingly.

Because we want to operate the target 3 degrees sub-cooled to minimize local boiling, the return temperature of the coolant should be 19K. The required He gas mass flow is therefore

$$\dot{m} = \frac{2100 W}{(6.26 J/gK)(19^\circ - 15^\circ)} = 84 g/s, \quad (12)$$

considerably higher than the approximately 30 g/s maximum 15K flow rate the ESR is capable of delivering. Figure 12 shows how we propose to overcome these limitations in our preferred refrigeration option. Rather than trying to obtain higher mass flow, the required cooling power can be obtained by lowering the coolant supply temperature from the nominal 15K provided by the ESR. The most cost-effective way to do this is to utilize the 4K coolant from the CHL in a new heat exchanger whose function is to lower the ESR 15K coolant temperature to about 8K. Figure 13 indicates that with an 8K supply temperature, we would require about 30 g/s mass flow from the ESR. This is only slightly larger than the mass flow that was achieved to operate the Hall A target at about 700W in Figure 11. We estimate this simple solution would cost \$25K

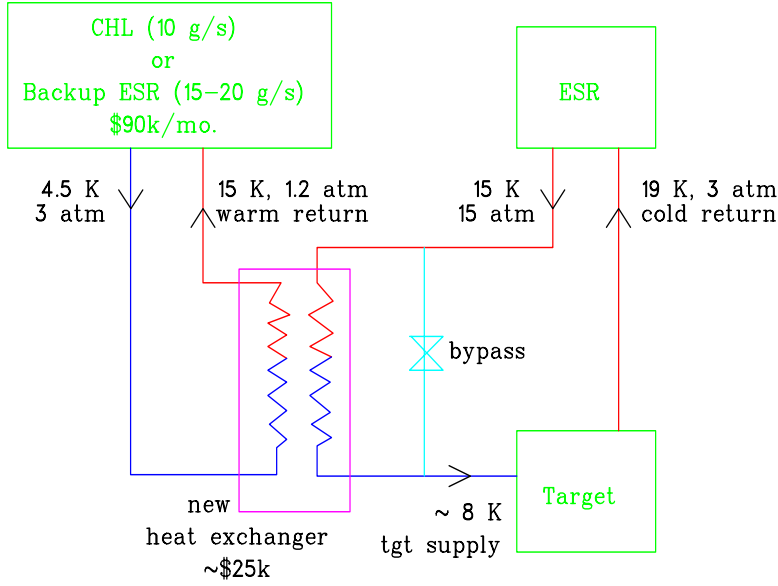


Figure 12: Schematic showing the proposed solution to obtain 2 kW of coolant for the target.

to implement. It would give us the cooling power needed for the  $Q_{weak}$  target without the cost, leadtime, or schedule uncertainty associated with other two options.

### 3.3.2 Density variations

We have studied several possible target concepts based on the above design parameters. In doing so we have considered the local temperature rise  $\Delta T$  of the  $LH_2$  in the path of the beam:

$$\Delta T = \frac{\Delta E (J/cm)}{m_l (g/cm) C_p (J/gK)} \quad (13)$$

$$= \frac{dE/dx (MeV/g/cm^2) I (\mu A) [A_{flow} (cm^2) = V_{vol} (cm^3/s) / v_s (cm/s)]}{d (cm) C_p (J/gK) V_{vol} (cm^3/s)} \quad (14)$$

where  $\Delta E$  is the beam energy deposited per cm of target length,  $m_l$  is the target mass along the beam axis,  $dE/dx$  is the beam ionization energy loss,  $I$  the beam current,  $A_{flow}$  the flow area across the beam axis,  $V_{vol}$  the volume flow provided by the recirculation fan,  $v_s$  the stream velocity transverse to the beam axis,  $d$  the raster width perpendicular to the flow direction, and  $C_p$  the specific heat of Hydrogen. The only way to decrease the local temperature rise is to either increase the raster size or increase the stream velocity.

In order to keep helicity correlated density fluctuations of the target at the level of 3% of the expected parity signal of  $3 \times 10^{-7}$ , we need to keep the helicity correlated  $\Delta T$  less than about  $6 \times 10^{-7} K$  (since  $\Delta \rho / \rho \sim -1.5\% \Delta T$ ). Assuming the charge asymmetry in the parity-quality beam at JLab is  $10^{-6}$ , which is what HAPPEX obtained, and solving the above equation for the stream velocity, we find that we need  $v_s \geq 700$  cm/s. This is the predicted flow velocity for the  $G^0$  target. To reduce the helicity correlated density fluctuations to a level where they do not

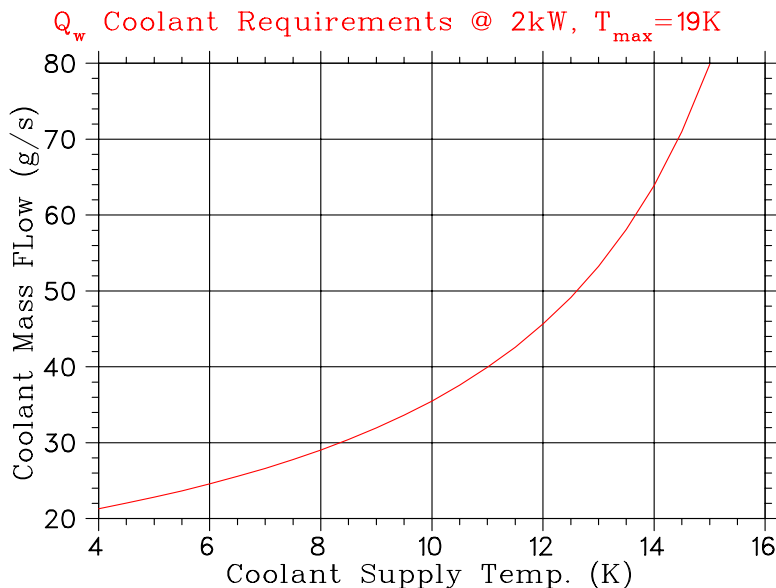


Figure 13: The coolant supply temperature is plotted against the required mass flow to achieve 2KW of cooling power for a 19K target.

contribute at all to the experimental uncertainty, we need to either maintain a charge asymmetry better than about  $2 \times 10^{-7}$ , or else calculate and correct for the density fluctuations to  $\leq 20\%$ , which is no problem.

Beyond these considerations, it is important to ensure the target does not boil and thereby introduce noise into the asymmetry measurements. Using the above equation with  $v_s = 700$  cm/s,  $I = 180 \mu A$ , and a  $2 \times 2 mm^2$  raster, we obtain  $\Delta T = 0.6K$ . Since we normally run 3 degrees sub-cooled (at 19K and 22 psia), the target fluid will not boil in the beam path.

### 3.3.3 Cryotarget design and cost estimate

Taking the above considerations into account, the target concept of choice for the  $Q_{weak}$  experiment is the SAMPLE/ $G^0$  design as illustrated in Figure 14. A high flow velocity is achieved by means of a perforated tapered cylindrical windsock, concentric to an outer cell. The flow area depends on the gap between the windsock and the target cell, as well as their respective radii, and the perforations. As a result the flow area can be made arbitrarily small and is almost independent of the length of the target. The small flow area inherent in this design contributes to the high flow velocity required by  $Q_{weak}$ . A flow velocity of 500 cm/s (at a circulating fan rate of 30 Hz) was achieved by the SAMPLE target, and as noted previously the  $G^0$  target flow velocity is designed to be 700 cm/s (also at 30 Hz). Although it would seem that these large flow velocities are moot since most of the net flow is longitudinal to the beam axis, in fact the high degree of turbulence produces a great deal of transverse diffusion.

The experience gained with the  $G^0$  target will carry over to this experiment, however, significant changes need to be made. The target cell itself will need to be lengthened from 20 to

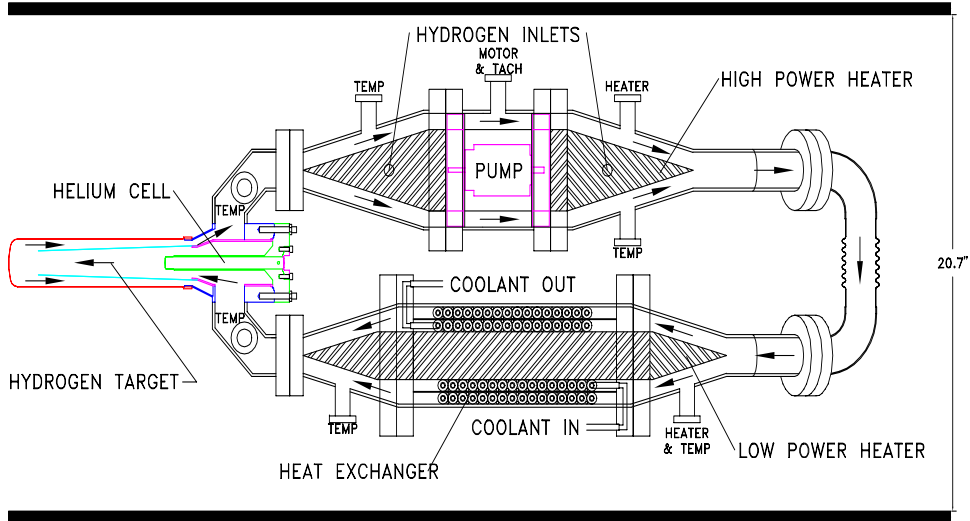


Figure 14: Schematic view of the  $G^0$  cryotarget. The  $Q_{weak}$  target will be somewhat similar but with a longer 35cm target cell.

35 cm. In addition the heat exchanger and heater capacity will need to be increased. Whereas the SAMPLE and  $G^0$  targets share many characteristics, they do have important differences in the pump location, heat exchanger design and orientation, and target cell diameter (which has implications for sensitivity to beam halo). From preliminary discussions with the JLab target group leader, M. Seely, we think the  $Q_{weak}$  target should be based more upon SAMPLE design choices (external motor, vertical loop, large target cell diameter), but with a heat exchanger similar to that used by standard JLab targets and the  $G^0$  target. The target end-windows may be fabricated from Beryllium rather than Aluminum to reduce background.

The impact of impurities in the  $LH_2$  on the  $Q_W^p$  measurement has been estimated. Contamination by heavier nuclei such as Helium or water ice must be limited to 0.1% by mass. Assuming an error-free fill of the gas system from a high purity bottle, we routinely find that the contamination of our  $H_2$  (principally by  $D_2$  or  $HD$ ) is  $0.1 \pm 0.1\%$  vol/vol. The major *measured* contaminant is  $N_2$  at only 10 ppm, which would not pose a significant problem for the  $Q_W^p$  measurement. However, we need to maintain good quality control at the gas panel and verify gas purity both before and after a run.

A cost estimate for the  $Q_{weak}$  cryotarget can be derived from the cost of the  $G^0$  target, since the designs are somewhat similar. The  $G^0$  target budget was originally \$230K. Factoring in the additional cost of the vacuum vessel and custom cryo-motors, the total  $G^0$  target cost will become \$300K. If a new CHL/ESR heat exchanger is needed for 2.1 kWatt operation, the cost will increase by \$25K to a total of \$325K. This is the number which appears in the Cost and Schedule Table 7.

## 3.4 High Current Beam

### 3.4.1 Technical feasibility from the injector viewpoint

The beam current of  $180\ \mu\text{A}$  proposed for this experiment is higher than has previously been employed for any single experiment at JLab. However, beam currents as high as  $140\ \mu\text{A}$  have already been delivered to Hall A for physics production, and based on past experience with the JLab polarized source guns, it should be possible to deliver  $180\ \mu\text{A}$  to Hall C at high beam polarization ( $>70\%$ ) for this experiment.

To deliver an average current of  $180\ \mu\text{A}$  to Hall C at the normal Hall repetition rate of 499 MHz, about  $300\ \mu\text{A}$  must be extracted from the photocathode, because the transmission through the injector apertures A1/A2 and the chopper master slit is only 60%. This gun current requirement is similar to the conditions of JLab Winter 2000 operations when  $\sim 250\ \mu\text{A}$  were extracted at high polarization from the gun for 2 months during simultaneous high luminosity running in Halls A and C (for the  $G_E^p$  and Madey/Kowalski  $G_E^n$  experiments, respectively). At that time, a photocathode “ $1/e$  lifetime” of roughly 300 Coulombs was observed. Assuming a similar photocathode lifetime, an initial photocathode quantum efficiency of typically 0.15%, and 500 mW laser power from a Ti-sapphire laser,  $180\ \mu\text{A}$  could be maintained into Hall C for roughly 11.5 days before the quantum efficiency dropped too low to provide the requested beam current. At that point the laser spot could be moved to a fresh location (20 minutes downtime) or, assuming all “spots” were exhausted, one could make an injector access to heat and reactivate the photocathode (an 8 hour process). The latter is ideally done only on maintenance days.

Of course we must also consider the beam current requirements of the other halls. For example, if Hall A were to request  $100\ \mu\text{A}$  at the same time, the photocathode lifetime would certainly decrease compared with the numbers mentioned above. In such a situation, it would be necessary to extract  $\sim 450\ \mu\text{A}$  from the gun ( $300\ \mu\text{A}$  for  $Q_{weak}$  plus  $150\ \mu\text{A}$  for Hall A). This would necessitate more frequent spot moves and cathode reactivations, but does not appear to be a problem. While JLab admittedly has no experience running the gun at  $450\ \mu\text{A}$ , the injector space charge effects (which are proportional to the square of the bunch charge) are an order of magnitude smaller for the standard 499 MHz  $Q_{weak}$  rep rate as compared to the 499/16 MHz rep rate of the upcoming  $G^0$  experiment.

Two developments may help improve the effective operating lifetime of the polarized injector. First, the JLab source group plans (independent of the  $Q_{weak}$  experiment) to increase the output power of the Ti-sapphire laser from 500 mW to 2 W. Such an increase will prolong the lifetime of the gun by a factor of 4. Second, they expect to become more adept at switching between polarized guns. A spare gun not only effectively doubles the operating lifetime of the photocathode between reactivations, but provides an alternative in the event that the first photocathode suffers from low polarization.

### 3.4.2 Miscellaneous administrative limits

Various other limits, including the beam dump current density limit, the site boundary dose, etc., are discussed in Appendix C.

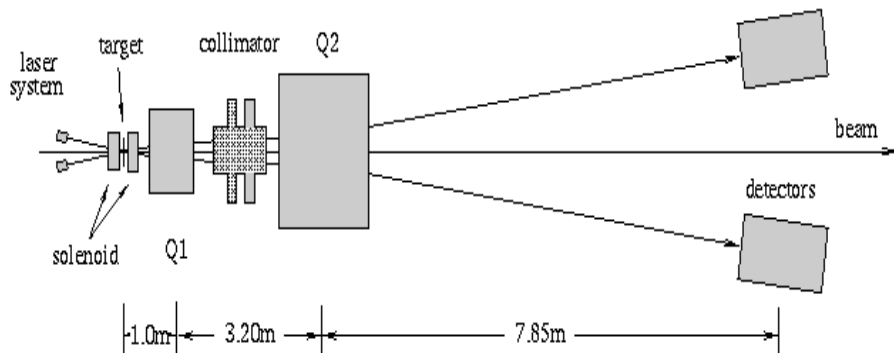


Figure 15: Layout of the Hall C Møller polarimeter. Note especially the superconducting solenoid which is used to drive the pure iron target foil into saturation. The magnetic field and the foil are oriented perpendicular to the beam.

### 3.5 Beam Polarimetry

The  $Q_{weak}$  experiment requires that the beam polarization be measured with an absolute uncertainty in the 1%-2% range. This is probably the single most challenging aspect of the experiment. In principle, the technology to do this already exists in Hall C in the form of the University of Basel Møller polarimeter [52], which provides an accurate absolute polarization measurement but is limited to operation at low beam currents ( $I_{beam} < 8\mu A$ ) and therefore cannot be run concurrently with parity data taking. While the Møller polarimeter will provide a very important capability for the  $Q_{weak}$  experiment, the collaboration also plans to build a Compton polarimeter to provide a continuous, relative monitor of the beam polarization during the high current production running.

#### 3.5.1 University of Basel Møller polarimeter in Hall C

While the standard  $e\bar{e} \rightarrow ee$  scattering process near  $\theta_{CM} = 90^\circ$  is used in the existing Hall C Møller polarimeter, its hardware configuration incorporates several significant improvements over previous devices of this type. A superconducting solenoid with a 4 Tesla, beam-axial field is used to drive a pure Fe target foil into saturation (See Figure 15), since the relationship between magnetization and electron polarization is best known for pure Fe. Coincidence detection eliminates most backgrounds, and the collimator design minimizes the effects of atomic Fermi motion in the target. A Monte Carlo program is used to determine the effective analyzing power of the apparatus, taking into account magnet and collimator positions and finite solid angles.

The University of Basel Møller polarimeter has been used to measure the polarization of

beam currents of several  $\mu A$  with an absolute accuracy of better than 1.5%. Unfortunately, the low beam current restriction is unavoidable, since it is necessary to avoid significant heating and therefore depolarization of the iron foil. Experience from the last several years suggests that lowering the beam current for dedicated Møller runs can introduce systematic errors at the 1%-2% level if great care is not taken. For example, reducing the beam current by closing the chopper slit can change the average polarization since the beam has a polarization profile. This problem can be eliminated by using the laser light attenuator to adjust the beam current rather than the chopper slit. However, since the  $Q_{weak}$  experiment will run at the elevated beam current of  $180\mu A$ , we will need to understand what happens to the beam polarization when the filter wheel attenuates the laser light by a factor of 30 [53].

Part of the  $Q_{weak}$  collaboration's polarimetry effort will go into determining whether modifications to the Basel Møller polarimeter target can enable it to operate at higher currents while retaining high accuracy. For example, if the Møller polarimeter could be made to work accurately at  $18.0\mu A$ , this would "only" be a factor of 10 below the production current. Even higher operating current for the Møller polarimeter cannot yet be ruled out: methods such as actively cooling the target frame, employing quasi-CW beam with for example 10% duty factor, and using the thinnest possible free-standing Fe foils will be explored.

### 3.5.2 Compton polarimeter

Clearly the  $Q_{weak}$  experiment will require a continuous, relative monitor of the beam polarization during the high current production running. The absolute accuracy of this polarimeter need not be high, as long as an accurate calibration can be transferred from the Basel Møller polarimeter. One possibility under serious consideration by the collaboration is to use a Compton polarimeter [54].

A Compton polarimeter takes advantage of the well-understood properties of Compton scattering of circularly polarized photons with longitudinally polarized electrons. The cross section differential in the energy  $E_\gamma$  of the scattered photon is given by

$$\frac{d\sigma}{dE_\gamma} = \frac{d\sigma_0}{dE_\gamma} (1 + P_\gamma P_{e,z} \alpha_{3z}(E_\gamma)), \quad (15)$$

where  $d\sigma_0/dE_\gamma$  is the Compton cross section for unpolarized photons and unpolarized electrons,  $P_{e,z}$  is the (longitudinal) polarization of the incident electron beam,  $P_\gamma$  is the degree of circular polarization of the light, and  $\alpha_{3z}$  is the circular-longitudinal spin correlation function [55].

The asymmetry in the cross section for the two different helicity states of the electron is proportional to the polarization of the beam:

$$A(E_\gamma) = \frac{\sigma^+ - \sigma^-}{\sigma^+ + \sigma^-} = P_\gamma P_{e,z} \alpha_{3z}(E_\gamma). \quad (16)$$

The degree of circular polarization  $P_\gamma$  must be measured independently. The  $\alpha_{3z}$  factor is calculable from Quantum Electrodynamics.

To minimize measurement times in determining the electron beam polarization with high precision, a high-gain resonant laser cavity can be used, similar to that used in the Hall A Compton Polarimeter [56]. Here, the laser cavity is built around the electron beam, such that

the probability for a laser photon to interact with the electron beam has effectively been increased by the gain of the resonant cavity.

Our MIT collaborators are currently involved in the construction of a Compton polarimeter for the Mainz A4 parity violation experiment. At 855 MeV and 20  $\mu\text{A}$ , Compton polarimetry measurements are an order of magnitude more difficult than for the  $Q_{weak}$  conditions. There is also a new Compton polarimeter being commissioned at MIT-Bates for the South Hall Ring BLAST experiment. Clearly, MIT is rapidly acquiring expertise in Compton polarimetry. Provided the  $Q_{weak}$  experiment is approved, they have proposed to build a Compton polarimeter for Hall C, working with other interested groups from the  $Q_{weak}$  collaboration.

Furthermore, in a JLab/Hampton/Virginia/Oregon State collaboration a resonant four-mirror cavity has been designed with a nominal gain of over 10,000, using an Ar-Ion laser at 514.5 nm. Fast feedback electronics has been built by the Fast Electronics group (according to NIST designs), and the resonant cavity has been operated in a JLab test setup with gains over 1,000 (4,000 with our optics and electronics at NIST). We note that the cavity is extremely robust. E.g., bouncing on the laser table will result in a short flicker of the cavity output, but the feedback restores the cavity performance within a second [61]. We have also performed measurements to characterize the mirror degradation due to the CEBAF accelerator environment, and have found a factor of 2 degradation in the mirror performance after a 230  $\mu\text{A}$ -day beam period. As the mirror reflectivity would allow for a nominal gain of  $\approx 30,000$ , and we assume only a gain of 1,000 for this experiment, the mirrors would not need to be replaced for at least one week of continuous running.

For this experiment, operating at a beam energy of  $\approx 1.2$  GeV, with a beam current of 180  $\mu\text{A}$ , use of an Ar-Ion laser (with wave length of 514 nm) would result in an asymmetry of 2.5%. Assuming a 1.8W laser power, a four-mirror cavity gain of 1,000 (with a length of 86 cm), a crossing angle of 3.38 degrees, and a Compton-backscattered photon detector with 1 mr acceptance, a 1% determination of a 70% polarized electron beam would require an  $\approx 10$  minute measurement. Frequency-doubling the Ar-Ion laser, to reduce systematical uncertainties by increasing the physics asymmetry, does not seem to be a reliable option yet, with state-of-the-art laser and mirror technology [62].

We propose to install a Compton Polarimeter in between the two legs of the Møller Polarimeter in the Hall C beam line. We will use a three-magnet dogleg system to induce a small bend in the electron beam and to resteer the beam back into the original beam line, as in Fig. 16. The 86 cm long laser cavity will interact with the electron beam just after the first bend. We will use an “extended-head” green Argon-Ion laser capable of delivering 1.8 W in single-line, single-mode configuration. The “extended head” option will allow us installation of a Gsanger EOM within the laser cavity. Such a laser has been quoted by Coherent Inc. for \$75K. One would be able to obtain also a 5 W laser power in single-mode, single-frequency (at 514.4 nm) for \$125K.

Note that a similar four-mirror Compton Polarimeter could function as a multi-purpose beam polarimeter device for Hall C in the energy range of 0.8 to 12 GeV/c.

The collaboration foresees two Research and Development projects concerning the Compton Polarimeter.

We consider changing the present design from a four-mirror resonant cavity to a two-mirror resonant cavity, with the two mirrors installed in precisely-machined metal holders as in the Hall

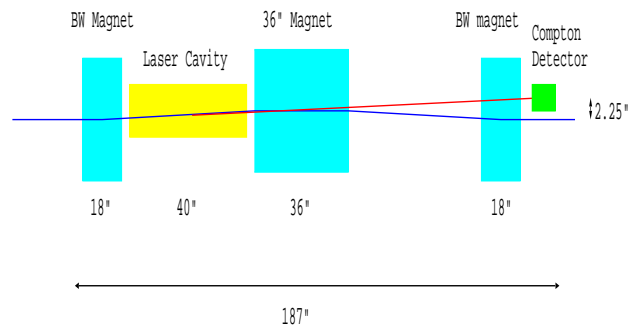
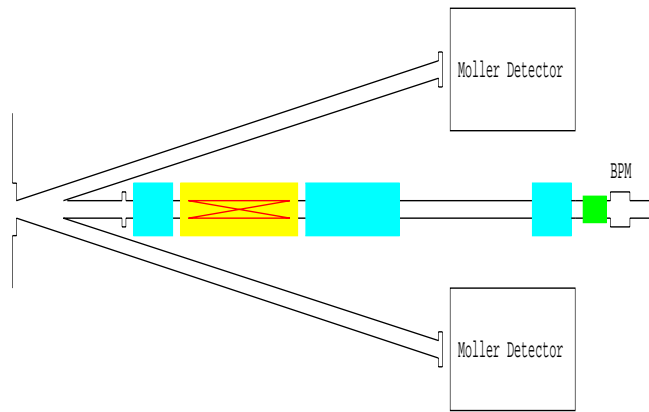


Figure 16: Sketch of the suggested three-magnet dogleg Hall C Compton polarimeter in between the Møller detector arms.

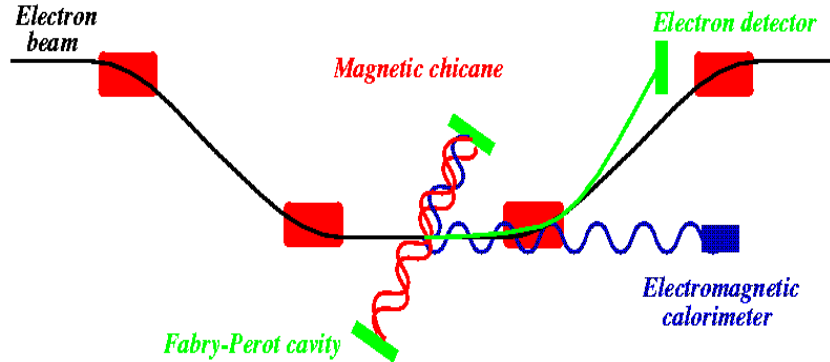


Figure 17: Schematic diagram of the Hall A Compton polarimeter. Figure taken from [57].

A Compton Polarimeter design. Our present design allows for a higher possible gain. However, the Hall A design would be more “user-friendly” and require far less alignment than a four-mirror cavity. The assumed cavity gain of 1,000 is rather modest and can easily be reached with the Hall A two-mirror design.

Furthermore, we have not conclusively decided between a four-magnet chicane, similar as the Hall A Compton polarimeter (see a schematic diagram in Fig. 17) rather than the mentioned three-magnet dogleg system. The three-magnet dogleg system seems far simpler, and can be accomplished with standard accelerator-type magnets, for which the design is readily available. The disadvantage may be that the space for photon detectors is limited, and that the mirrors may be more sensitive to electromagnetic background produced during Møller runs.

### 3.6 Statistical Error and Random Noise

Ideally, the statistical error in this experiment should be solely determined by the fluctuations in the number of detected electrons due to Poisson counting statistics. However, there are other sources of random noise that can contribute to the statistical error. In this section, we discuss how small these other sources must be to insure that we achieve the counting statistics limit.

In this experiment, we intend to integrate the detector signals for 33.333 msec periods. Between these periods, the beam helicity will be reversed in a pseudo-random way. The experimental asymmetry is formed from helicity “pulse pairs” of two of these periods. The raw experimental

asymmetry is given as:

$$A = \frac{Y_+ - Y_-}{Y_+ + Y_-} \quad (17)$$

where  $Y$  is the total integrated detector signal normalized to incident beam charge. The statistical error in the determination of  $A$  for each pulse pair arising from counting statistics can be written as:

$$\Delta A_{count} = \frac{1}{\sqrt{2}} \frac{1}{\sqrt{N_{e-}}} \sqrt{1 + \left(\frac{\sigma_{N_{pe}}}{N_{pe}}\right)^2} \quad (18)$$

Here,  $N_{e-}$  is the total number of scattered electrons detected per 33 msec integration period.  $N_{pe}$  is the average number of photoelectrons generated in the Čerenkov detector per scattered electron.  $\sigma_{N_{pe}}$  is the standard deviation of the distribution of photoelectrons per event; in our case it is dominated by the variation in collection efficiency for events in different parts of the Čerenkov detector. The expected value of this parameter from the current detector design is  $\sigma_{N_{pe}}/N_{pe} = 0.12$ . The expected count rate for the entire detector is 6.1 GHz. This corresponds to  $2.0 \times 10^8$  detected scattered electrons per integration period. These numbers result in:

$$\Delta A_{count} = 5.0 \times 10^{-5} \quad (19)$$

for the counting statistics error per pulse pair. Other sources of random noise should be kept small compared to this. These other sources of noise will add in quadrature with the above number. These other sources of noise include:

1. **Electronic noise in beam charge detection:** The incident electron beam charge is determined from resonant microwave cavity monitors. Signals from these devices are downconverted, amplified, and then digitized with voltage-to-frequency converters fed into scalars. Fluctuations in the incident beam charge will be taken out when the normalized detector yield is formed. However, random errors resulting from electronic noise in the circuitry and the finite precision of the beam charge measurement process will contribute to the random error in our measurement. A measurement of the random error in the charge measurement can be made by analyzing the readings from two nearby charge monitors with no aperture in between them. In the absence of random noise, there should be perfect agreement between the two; deviations from this quantify the noise level. A demonstration that the noise is at the required level will require higher frequency voltage-to-frequency converters than the 1 MHz ones in use now, due to the digitization “least-bit” noise at 1 MHz. We intend to use 10 MHz V-to-F’s for the  $Q_{weak}$  experiment, and then we can demonstrate that this noise is at the required level.
2. **Detector electronic noise:** Detector electronic noise will also contribute to the random error. As described in more detail in Section 3.2.2, the Čerenkov detector electronics is designed to keep this noise well below the counting statistics limit.
3. **Target density fluctuations:** Target density fluctuations on the timescale of the experimental integration time (33 msec) can also contribute to the random error. We require

that the fractional size of such target density fluctuations be small compared to our counting statistics limit of  $5.0 \times 10^{-5}$ . The target design discussed in Section 3.3 is aimed at achieving this.

## 3.7 Systematic Errors

### 3.7.1 Corrections due to helicity-correlated beam properties

Helicity-correlations in the beam parameters can lead to false asymmetries in the experiment. All parity-violating electron scattering experiments have dealt with this by making corrections to the measured asymmetry to account for the helicity-correlated beam properties. This can be written as:

$$A_{meas} = A_{phys} + \sum_{i=1}^N \frac{1}{2Y} \left( \frac{\partial Y}{\partial P_i} \right) \Delta P_i \quad (20)$$

where  $Y$  is the normalized detector yield and  $\Delta P_i = P_{i+} - P_{i-}$  is the helicity-correlated difference for beam parameter  $i$ . The detector sensitivities,  $\partial Y / \partial P_i$ , can be determined by occasional deliberate modulation of the relevant beam parameter or from the space spanned by the natural variation of the beam parameters. The helicity-correlated beam parameter differences,  $\Delta P_i = P_{i+} - P_{i-}$ , are measured continuously during data-taking. From estimates of the sensitivity of our experiment to beam parameter variations, we can set requirements on how accurately beam parameters have to be measured and how small the helicity-correlations in these parameters must be.

The first requirement is that the beam parameters be measured accurately enough so that the error on the correction made to the asymmetry be small. We require that the error on any individual correction is no greater than 10% of the statistical error. This requirement leads to the beam parameter measurement precisions tabulated in Table 2. In constructing this table, we made estimates for the detector sensitivities that take into account the collimator acceptance only, and we assumed that the acceptances of the individual detectors are matched to 1%. All of the measurement precision requirements listed in Table 2 have been achieved at Jefferson Lab. For example, the typical observed precision for beam position measurements at 15 Hz is 10  $\mu$ , and this is dominated by natural beam noise.

Table 2: Required accuracy for measurement of beam parameters so that the error due to the individual beam parameter correction is less than 10% of the  $Q_W^p$  expected statistical error.

Parameter	Accuracy required per 15 Hz pulse-pair
Beam energy	$\Delta E/E \sim 0.6 \times 10^{-5} \rightarrow 21 \mu\text{m}$ at 35 mm/% dispersion
Beam diameter at target	1 mm
Beam position at target	.38 mm
Beam angle at target	60 $\mu\text{rad}$ (1.2 mm at 20 m separation)

The second requirement is that the helicity-correlations in the beam parameters are kept small enough so that the individual corrections to the asymmetry are acceptably small. We require that the overall run-averaged correction for any beam parameter be no larger than the size of the statistical error. This leads to the requirements listed in Table 3 for the run-averaged helicity-correlated beam parameter differences. We note that the 1999 HAPPEX experiment that used the strained GaAs crystal was able to keep the run-averaged position differences below the 50 nm level. By the time  $Q_{weak}$  runs, there will be a helicity-correlated position feedback system that should be in routine operation, so this number should improve.

Table 3: Requirements for the overall run-averaged helicity-correlated beam properties such that the correction to the asymmetry from that beam parameter is the same as the expected  $Q_{weak}$  statistical error.

Parameter	Run-averaged helicity correlation
Beam energy	$\Delta E/E \sim 1.0 \times 10^{-8}$ 35 nm at 35 mm/% dispersion
Beam diameter at target	1.7 $\mu\text{m}$
Beam position at target	.6 $\mu\text{m}$
Beam angle at target	60 nrad (1.2 $\mu\text{m}$ at 20 m separation)

The conclusion is that our requirements for helicity-correlated beam properties are no more stringent than conditions that have already been achieved for parity-violation experiments at Jefferson Lab.

### 3.7.2 Determination of average $Q^2$

Since the parity-violating asymmetry is proportional to  $Q^2$ , it is critical to determine the average  $Q^2$  for the electrons from the  $ep$  elastic scattering events of interest with  $\simeq 1\%$  accuracy. The absolute beam energy will be known to  $\leq 0.1\%$  using the Hall C energy measurement system. The central scattering angle for each collimator will be determined by redundant survey techniques to  $\leq 1$  mrad. Over short baselines, the JLab alignment group routinely achieves this accuracy. As was the experience from the HAPPEX experiment [31], angle errors will dominate the error in  $Q^2$ . In particular, the error for our kinematics is approximately 1.4%/mrad. The carefully measured target and collimator geometries relative to the electron beamline will then define the  $Q^2$  bite in a simulation which properly accounts for radiative and multiple-scattering effects.

This is an integrating experiment, so determination of the average  $Q^2$  has further complications. The  $Q^2$  dependence of the  $ep$  cross section will bias the average detected  $Q^2$ . This and any position-dependent detector bias must be taken into account (since  $Q^2$  may be correlated with position at the focal plane). Although in principle these matters can be simulated, it is important to check the experiment Monte Carlo using ancillary measurements: one to measure the shape of the focal plane distributions, and another to measure the position-dependent detector bias.

Careful thought needs to go into the choice of survey techniques. Furthermore, since survey

and alignment are critical, it is important that the experiment be designed from the outset such that the beamline, cryotarget, and collimators can be accurately and redundantly surveyed.

### 3.7.3 Nucleon form factor contributions

As shown in Equation 10 of Section 2.3, the asymmetry expression contains contributions from nucleon structure form factors. They increase in relative importance as one moves away from  $Q^2 = 0$ . To consider the impact of these contributions on our measurement, we write the asymmetry as follows:

$$A = A_{Q_W^p} + A_{nff} + A_{axial} \quad (21)$$

The first term involves the quantity of interest,  $Q_W^p$ . The second term involves the electromagnetic and strange nucleon form factors. It reduces to the  $Q^4 B(Q^2)$  term in Equation 10 for small  $Q^2$ . The third term involves the e-N axial form factor  $G_A^e$ . Both the second and third terms depend on nucleon structure form factors, but we exhibit them separately because they have different kinematic dependences.

The term  $A_{nff}$  can be constrained from the anticipated results of parity-violating electron scattering experiments that will be performed at Jefferson Lab in the next few years. These experiments will be performed at higher  $Q^2$  values than  $Q_{weak}$ , so we must extrapolate to determine the value of  $A_{nff}$  at our  $Q^2$ . In Figure 18, we show the published uncertainty from HAPPEX [35] and the expected uncertainties from HAPPEXII [36] and the forward angle running of  $G^0$  [37]. To extrapolate, we must assume a functional form for the  $Q^2$  dependence of  $A_{nff}$ . For this extrapolation, we assume conventional dipole and Galster parameterizations for the electric and magnetic proton and neutron form factors. For the electric and magnetic strange form factors,  $G_E^s$  and  $G_M^s$ , we use two different functional forms that have been proposed in the theoretical literature. The functional forms assumed are the conventional dipole and Galster [33] and the prediction of a lattice gauge theory calculation [34]. The free parameters in the extrapolation are the strange magnetic moment ( $\mu_s \equiv G_M^s(Q^2 = 0)$ ) and the strangeness radius ( $r_s^2 \equiv -6[dG_E^s/dQ^2]_{Q^2=0}$ ). In Figure 18, we show the range of values of  $A_{nff}$  that can be accommodated at the  $1\sigma$  confidence level for the different assumptions about strange form factor  $Q^2$  dependences.

From Figure 18, the fractional uncertainty on  $A_{nff}$  is  $\pm 4.0\%$  at  $Q^2 = 0.03 \text{ GeV}^2$ . At our kinematics,  $A_{nff}$  contributes 40% to the asymmetry. Thus, this leads to a 1.6% uncertainty arising from our expected knowledge of electromagnetic and strange nucleon form factors.

The axial contribution,  $A_{axial}$ , depends on the e-N axial-vector form factor  $G_A^e$ . At tree level, this is known from neutron beta decay and neutrino scattering. However, this term also contains significant contributions from higher order electroweak corrections. This has been demonstrated both theoretically [38,39] and experimentally from the results of the SAMPLE experiment [40]. At  $Q^2 = 0.1 \text{ GeV}^2$ , the SAMPLE experiment found  $G_A^e = +0.22 \pm 0.45 \pm 0.39$  as compared to the theoretical prediction of  $G_A^e = -0.83 \pm 0.26$ . The errors on this quantity will be measured more precisely in an ongoing SAMPLE experiment [42] and from the  $G^0$  backward angle measurements [41]. After these measurements, it is expected that the extrapolated absolute error on  $G_A^e$  at  $Q^2 = 0.03 \text{ GeV}^2$  will be  $\pm 0.25$ . The  $A_{axial}$  term makes a 5% contribution to the overall asymmetry (assuming  $G_A^e = 1$ ) at the  $Q_{weak}$  kinematics, so there is a 1.2% error arising from the

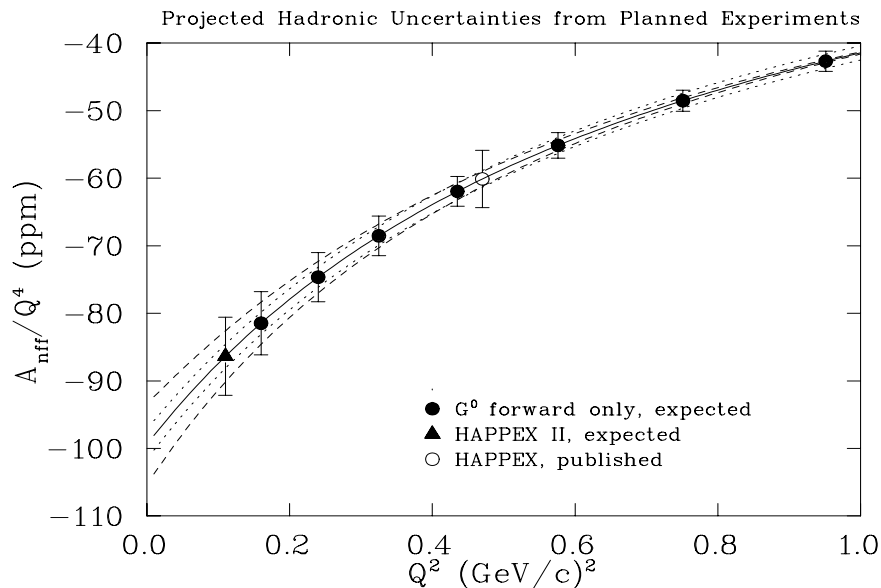


Figure 18: Projected hadronic uncertainties from Planned Experiments: the data points represent published or anticipated errors on  $A_{nff}/Q^4$ . The lines show the  $1\sigma$  range from fits under various assumptions about the strange form factor  $Q^2$  dependences. The dashed line corresponds to dipole/Galster [33] and the dotted line corresponds to lattice gauge theory [34]. The free parameters in each case are the strange magnetic moment,  $\mu_s$ , and the strangeness radius,  $r_s^2$ . The central solid line assumes the strange form factors are zero.

axial form factor.

The quadrature sum of the two above nucleon form factor errors is 2%.

### 3.7.4 Effects due to transverse polarization

If the electron beam has a non-zero transverse polarization component, then our experiment will be sensitive to the parity-conserving vector analyzing power arising from the interaction of the electron spin with the nuclear current in the electron's rest frame. For spin-0 nuclei this is referred to as the Mott asymmetry [58]. This is a parity-conserving left-right analyzing power, so it vanishes for a perfectly symmetric detector. As we show here, this is likely to be a very small effect in our experiment.

The Mott asymmetry formula [58] is known for spin-0 nuclei, and it has been extensively tested at low energies. However, for nuclei with non-zero spin at finite  $Q^2$ , there are no theoretical formulae for this asymmetry. There has been one measurement made by the SAMPLE collaboration at backward angles and  $Q^2 = 0.1 \text{ GeV}^2$  [59]. The observed value was about a factor of 3 smaller than what the simple Mott asymmetry formula predicts. Thus, we conclude that this formula is adequate for an order of magnitude estimate of this effect.

For the  $Q_{weak}$  kinematics, the Mott asymmetry formula predicts an asymmetry of 0.008 ppm for Hydrogen and 0.105 ppm for aluminum. We are considering beryllium as an alternate end window material; its Mott asymmetry is smaller than aluminum since the asymmetry is

proportional to  $Z$ . If we assume that there is a residual 5% relative transverse component in the JLab beam, and we assume that the acceptance of the focal plane detectors is matched to 1%, then the overall contribution to the asymmetry from this effect is about  $4.5 \times 10^{-6}$  ppm as compared to our expected parity-violating asymmetry of about 0.3 ppm. Thus, this is a very small effect. It is also possible to set a direct upper limit on this contribution by taking a short amount (about 1 day) of data with the beam polarization fully transverse. This would yield a direct upper limit on this contribution that is small compared to our expected statistical error.

### 3.7.5 Null tests

In parity-violation experiments it is useful to have “null tests” to check that asymmetry contributions that are expected to be zero are consistent with zero at the experiment’s level of statistical precision. One frequently used test of this type is the so-called “slow half-wave plate reversal”. The half-wave plate is an optical element inserted in the laser beamline in the polarized injector. Every few days it is inserted or removed. The effect is to reverse the sign of the electron beam’s helicity without making any changes to the electronic signals that define and record the beam helicity. True parity-violation effects should reverse sign under this operation. False effects correlated with the reversal signal will not reverse sign and can be distinguished with this technique.

Another possible null test that we will explore is the use of very forward angle detectors. This technique was used successfully during the SAMPLE experiment [60]. The idea is to place quartz Čerenkov detectors (like our primary  $Q_{weak}$  detectors) just outside the beampipe far downstream of our experiment at a scattering angle of about  $2^\circ$ . These detectors would primarily detect 450 MeV Møller electrons and elastically scattered electrons. The rates are such that the statistical precision per helicity pulse-pair would be much higher than the primary  $Q_{weak}$  detectors. On the other hand, the physics asymmetry from these processes is much smaller than the  $Q_{weak}$  asymmetry, so these provide a high precision “null-check” on the asymmetry. These detectors will have sensitivity to helicity-correlated beam motion, so they also provide a good test of the asymmetry corrections procedure. Finally, due to the high statistical precision of these detectors, they would detect any sign of target density fluctuations well before the primary  $Q_{weak}$  detectors.

## 3.8 Backgrounds

### 3.8.1 Backgrounds from target windows

The contamination of the elastic proton asymmetry from the scattering in 3.5 mil aluminum windows was estimated assuming nominal central kinematics. [43] Here we are referring to the windows through which the primary beam enters and exits the target cell. It was also assumed that it will not be possible to reject these backgrounds in our focal plane detectors. Both elastic scattering on the Aluminum nucleus and quasielastic scattering from the protons and neutrons in the Aluminum were considered. (Transitions to excited states of Aluminum, which may be important at  $Q^2 \simeq 0.030 (GeV/c)^2$ , have not yet been estimated.) The results are shown in Table 4. The relative contamination of the asymmetry of interest (elastic scattering from protons) is shown in the last column. Below, each of these processes is considered separately, and an estimate

is made of the systematic error associated with these processes using our theoretical knowledge of their asymmetries. We find that, although we can make reasonable estimates of the window backgrounds, the resulting uncertainties are not comfortably below our other errors. Therefore a dedicated window background measurement will be performed.

Table 4: Contributions of the various scattering processes in the Hydrogen target and the windows at the  $Q_{weak}$  central kinematics.  $t$  is the target thickness in particles/cm<sup>2</sup>,  $R_{cont}$  is the fractional contribution of the contamination to the rate in the detector, and  $A_{cont}$  is the contribution of the contamination to the overall asymmetry ( $=-0.27$  ppm) from that process. The relative contamination of the elastic proton asymmetry from each process is shown in the last column.

Process	$\sigma$ ( $\mu\text{b/sr}$ )	A (ppm)	t ( $\text{cm}^{-2}$ )	$R_{cont}$ (%)	$A_{cont}$ (ppm)	$\frac{A_{cont}}{(-.30)}$ (%)
Protons in $LH_2$ (elastic)	88	-0.31	$1.3 \times 10^{24}$	97.8	-0.30	
Protons in Al (quasi-elastic)	88	-0.31	$1.4 \times 10^{22}$	1.05	-0.0033	1.1
Neutrons in Al (quasi-elastic)	3	-3.1	$1.5 \times 10^{22}$	0.04	-0.0012	0.4
$^{27}\text{Al}$ nucleus (elastic)	1234	+3.0	$1.05 \times 10^{21}$	1.1	+0.033	-11.0

The detailed calculations for target window backgrounds are found in Appendix D. We summarize the discussion on window backgrounds here. For aluminum end window thicknesses of 3.5 mil (front and back), quasielastic and especially elastic backgrounds must be taken into account. For our kinematics, the elastic contribution from the windows is dominant. In particular, the contributions to the asymmetry could be as large as 3.3% from the quasielastic and 11% from the elastic scattering. These estimates are based on what is currently available in the literature regarding these processes.

The Aluminum background will be measured directly by using a special empty target cell with windows about 20 times thicker than the full target cell windows (to maintain the same radiation length). Assuming the rates in Table 1, and that the empty target cell can take full production beam current, it would take only 25 hours to determine the window asymmetry such that its contribution to the Hydrogen asymmetry error was at the 1% level.

In practice the indirectly cooled empty target cell windows are unlikely to withstand full production beam current, so we may have to allocate more time to the window background measurement. Clearly, we can do the experiment with Aluminum target windows. However, we still plan to investigate whether Beryllium would, for the same strength window, produce smaller backgrounds than Aluminum.

### 3.8.2 Backgrounds from other reactions

In addition to elastic scattering on the proton, there are several other processes that can take place in our target. Our spectrometer and detector are designed to accept, in principle, only the elastic scattering peak. However, other reactions can reach the detectors by rescattering (*e.g.*, on the face of the collimators or in the Helium gas). It is useful to know which background processes are potentially important by determining what fractional contamination can be tolerated before a significant error results in the  $Q_W^p$  measurement.

In Table 5, we list the various potential background processes, their cross sections, and their parity violating asymmetries at our mean scattering angle of  $9^\circ$ . Only single pion inelasticities up to the  $\Delta$  region have been considered. We also compute the maximum tolerable contamination of the elastic signal from each process such that they contribute  $< 1\%$  to the elastic scattering asymmetry. The reactions are separated into those which produce positively and negatively charged particles. Positive particles are suppressed by an enormous factor by the bend direction of the magnetic field. Negative particles are suppressed by the elastic focus and the requirement to have sufficient rigidity to cross the magnetic field. Production of neutrals has not been examined yet because the detector is very insensitive to neutrons and because of the small large-angle rescattering probability for gammas. Assuming the electrons from Møller scattering have too low a rigidity to make it to the focal plane, the reaction of greatest concern is inclusive  $p(e, e')X$  for which the allowable contamination is only  $1\%$ . However, given the relatively small cross section for inclusive pion electroproduction ( $\sigma_{el}/\sigma_\pi \simeq 10$ ) and the large separation between the elastic events and pion threshold at the detector plane, we expect the contamination from pion electroproduction will be negligible.

We plan to follow up on these estimates with a full GEANT simulation to examine the effects of rescattering of charged and neutral products. This will allow us to design the experiment so as to minimize the contamination from other reactions. It is also important to try to measure these effects during the experiment. This can be done by changing the QTOR field to focus, in turn, the super-elastic and the pion threshold regions onto the detector plane to measure their PV asymmetries.

### 3.8.3 Signal-to-background dilution factor

The physics asymmetry in our experiment will be diluted by the signal-to-background dilution factor,  $S/(S + B)$ , where  $S$  is the signal due to elastic scattering on Hydrogen and  $B$  is the background due to other processes. This is a dilution factor just like the beam polarization, and it must be known with good relative precision (about  $1\%$ ).

Our detector is designed to be insensitive to everything except elastic scattering on Hydrogen. However, there is a direct measurement we can do to convince ourselves that we have adequately suppressed other background processes. The elastically scattered electrons will be the only reaction product that can make it through our collimation system with momentum near that of the beam. The typical elastically scattered electron will have a momentum of 1145 MeV. In our normal data-taking mode, we will integrate the detector signal, so we cannot accumulate an energy spectrum. To determine the energy spectrum, we can turn down the incident beam current low enough to allow the counting of individual pulses in our Čerenkov detector. If we then back

Table 5: Cross sections and asymmetries for processes in the Hydrogen target at the mean scattering angle of  $9^\circ$ . The final column,  $F_{cont}^{max}$ , shows the maximum tolerable fractional contamination so that the given process will contribute less than 1% to the elastic scattering asymmetry.

Process	Reaction	$\sigma$ ( $\mu\text{b}/\text{sr}$ )	$ A $ (ppm)	$F_{cont}^{max}$ (%)
<b>Negative products:</b>				
Elastic $e^-$	$p(e, e)p$	88	0.31	
Møller $e^-$	$e(e, e)e$	80000	.0006	.6%
Inclusive $e'$	$p(e, e')X$	8.7	3.3	1%
<b>Positive products:</b>				
Recoil $p$	$p(e, p)e$	.0001	117	2300% (OK!)
$\pi^+$ Electroproduction	$p(e, \pi^+)en$	0.3	160 (max)	.6%
$\pi^+$ Photoproduction	$p(\gamma, \pi^+)n$	0.5	<1	50%

part of this detector with a small electromagnetic calorimeter array with good (3-4%) resolution, we can make a measurement of the energy spectrum of the particles that deposit a signal in our Čerenkov detector. Combining this information with the photoelectron spectra from our Čerenkov detector will allow us to determine accurately the fraction of our “integration-mode” signal that is due to elastically scattered electrons.

### 3.9 Total Error Budget

We have outlined a competitive measurement of  $Q_W^p$  with combined statistical and systematic errors of approximately 4% as given in Table 6.

To put our experiment in perspective, the  $Q_W^p$  physics asymmetry is slightly smaller than the already approved JLab neutron radius measurement E00-003 (.3 ppm versus .5 ppm) with a slightly smaller statistical error (2% versus 3%).

Table 6: Total error budget for the experiment. Note that due to the dilution by hadronic form factor effects, a 1% error on the asymmetry due to the uncertainty in beam polarization, for example, yields a 1.4% error in  $Q_W^p$ .

<u>Source of error</u>	<u>Contribution to <math>\Delta Q_W^p / Q_W^p</math></u>
Statistical error	2.8%
Hadronic structure	2%
Absolute $Q^2$ determination	1%
Beam polarimetry	1.4%
Target window background	1%
<b>TOTAL:</b>	<b>4.0%</b>

## 4 Cost and Schedule

An estimate for the cost and schedule of the  $Q_{weak}$  experiment appears in Table 7.<sup>34</sup> From JLab's point of view, the  $Q_{weak}$  effort may fit nicely in a window between  $G^0$  activities in the near term, and 12 GeV upgrade activities in the longer term. However, from the collaboration's point of view, a fast-paced effort to fund, design, and construct the  $Q_{weak}$  apparatus will begin as soon as we receive PAC approval.

Table 7: Cost and schedule for the  $Q_{weak}$  experiment in K\$. We expect the project to be funded by a combination of NSF, DOE, and NSERC grants to user institutions, as well as a significant contribution from JLab and LANL. The total DOE equipment cost will be less than \$2M. We have not included resources associated with installation which are typically provided for major installation experiments by JLab.

	<u>Year 1</u>	<u>Year 2</u>	<u>Year 3</u>	<u>Year 4</u>	<u>Year 5</u>	<u>Total</u>
				First Run	Production Run	
<b>R&amp;D:</b>	100					100
<b>Construction:</b>						
Magnet and P.S.		300	300			600
Detectors		125	225			350
Electronics		50	50			100
Target System		150	175			325
Calibration Equip.	50	75	75			200
Lum. Monitor		25	25			50
Collimators		50	50			100
Shielding	100	100	100			300
Data Acquisition			25			25
Polarimeter						
Beamline				75		75
<b>Total Cost by Year</b>	<b>300</b>	<b>825</b>	<b>1025</b>			<b>2225</b>

<sup>3</sup>The Møller polarimeter already exists as discussed earlier. A new Compton polarimeter is part of the internally planned Hall C upgrade program, and as a general purpose device is not included in our cost estimate.

<sup>4</sup>Our plan is to use the  $G^0$  beamline and instrumentation essentially as is. The budget contains \$75K for minor modifications to that system.

Table 8: Example of a hypothetical cost breakdown by funding agency and laboratory.

	<u>Year 1</u>	<u>Year 2</u>	<u>Year 3</u>	<u>Year 4</u>	<u>Year 5</u>	<u>Total</u>
NSERC (Canada)		150	150			300
NSF		200	300			500
DOE		275	300			575
JLab	150	300	325	75		850
LANL						
Total						2225

## 5 The Collaboration

Members of the  $Q_{weak}$  collaboration have extensive experience in parity violating measurements with hadronic probes at LANL and TRIUMF, and with electron beams at Bates, TJNAF, at Mainz. Strong theoretical support within the collaboration is provided by J. Erler and M. Ramsey-Musolf.

## 6 Beam Request

At this time we request approval for a first run of 23 days. The goal of the first run will be to check out the  $Q_{weak}$  apparatus, carry out systematic studies, make the first ever measurement of the proton's weak charge, and obtain a statistical error on  $\sin^2 \theta_W$  comparable to the SLAC E-158 PV Møller scattering measurement.

This first run would be preceded by facility development periods where, for example, 2.1 kW cooling power could be delivered to the target, followed by a later full power test of the target with beam. Parasitic and dedicated-user studies of the beam and various monitors will also precede the first run.

Provided we have demonstrated control of the systematics at the required level in the first run, we will make an additional beam request to bring the final combined statistical and systematic errors on  $Q_W^p$  to 4%. At that point the statistical and systematic errors would be roughly balanced. A total of 2200 hours will be required.

## 7 Summary

Herein the  $Q_{weak}$  collaboration has presented plans for the first Standard Model test at JLab. In contrast with the rest of the JLab physics program, this experiment is *not* designed to elucidate the physics of complexity in strong QCD. Rather, this experiment is designed to lift the obscuring veil of strong QCD, and so observe how leptons and quarks interact at low energies. This will be the first measurement of  $Q_W^p$ . As a search for new physics at low  $Q^2$ , this experiment is very competitive with the SLAC E-158 Møller scattering experiment. As a search for new physics at low energies in the semi-leptonic sector, the proposed experiment is to our knowledge without

equal. We believe the measurement is timely, the physics goals are meritorious and, moreover, achievable.

### Acknowledgements

We thank Nathan Isgur, Mark Sher, and Dirk Walecka for their helpful comments and suggestions. This work is supported in part by grants from the National Science Foundation and the US Department of Energy.

## References

- [1] C.Y. Prescott *et al.*, Phys. Lett. **B77**, 347 (1978).
- [2] C.Y. Prescott *et al.*, Phys. Lett. **B84**, 524 (1979).
- [3] The LEP Collaborations ALEPH, DELPHI, L3, OPAL, the LEP Electroweak Working Group and the SLD Heavy Flavour and Electroweak Groups: D. Abbaneo *et al.*, preprint CERN-EP-2001-021.
- [4] R.C. Carr *et al.*, “A Precision measurement of the weak mixing angle in Møller scattering”, SLAC proposal E-158 (1997); E. Hughes, K. Kumar, and P. Souder, spokespersons.
- [5] K. Kumar, private communication.
- [6] S.C. Bennett and C.E. Wieman, Phys. Rev. Lett. **82**, 2484, (1999); C.S. Wood *et al.*, Science **275**, 1759 (1997).
- [7] A. Derevianko, “Reconciliation of the measurement of parity-nonconservation in Cs with the standard model,” Phys. Rev. Lett. **85**, 1618 (2000)
- [8] W. R. Johnson, I. Bednyakov and G. Soff, “Vacuum polarization corrections to the parity-nonconserving 6s - 7s transition amplitude in Cs-133,” e-print hep-ph/0110262.  
A. I. Milstein and O. P. Sushkov, “Parity nonconservation in heavy atoms: The radiative correction enhanced by the strong electric field of the nucleus,” e-print hep-ph/0109257.
- [9] V. A. Dzuba, V. V. Flambaum and J. S. Ginges, “Calculation of parity nonconservation in Cesium and possible deviation from the standard model,” e-print hep-ph/0111019.
- [10] V. A. Dzuba and V. V. Flambaum., “Off-Diagonal Hyperfine Interaction and Parity Non-conservation in Cesium,” e-print physics/0005038.
- [11] NuTeV Collaboration: G. P. Zeller *et al.* “A Precise Determination of Electroweak Parameters in Neutrino-Nucleon Scattering,” e-print hep-ex/0110059.
- [12] For a review, see I. Hinchcliffe, Eur. Phys. J. **C 15**, 85 (2000)

- [13] TOPAZ Collaboration: I. Levine *et al.* Phys. Rev. Lett. **78**, 424 (1997);  
VENUS Collaboration: S. Odaka *et al.* Phys. Rev. Lett. **81**, 2428 (1998);  
OPAL Collaboration: G. Abbiendi *et al.* Eur. Phys. J. C **13**, 553 (2000);  
L3 Collaboration: M. Acciarri *et al.* Phys. Lett. B **476**, 40 (2000).
- [14] M. J. Ramsey-Musolf, Phys. Rev. C **60**, 015501 (1999)
- [15] Muon g-2 Collaboration: H. N. Brown *et al.* Phys. Rev. Lett. **86**, 2227 (2001).
- [16] P.A. Souder *et al.*, PRL **65**, 694-697 (1990).
- [17] CDF Collaboration: F. Abe *et al.* Phys. Rev. Lett. **79**, 2192 (1997).
- [18] V. Barger and K. Cheung, Phys. Lett. **B480**, 149 (2000).
- [19] K. Cheung, Phys. Lett. **B517**, 167 (2001).
- [20] D.H. Beck and B.R. Holstein, hep-ph/0102053, to be published in Int. J. Mod. Phys. E
- [21] M. J. Musolf *et al.*, Phys. Rep. 239., 1 (1994).
- [22] A Proposal for the Bates Large Acceptance Spectrometer Toroid, The BLAST Collaboration.
- [23]  $G^0$  Technical Design Report, Nuclear Physics Laboratory, University of Illinois at Urbana-Champaign, 1993.
- [24] “Basic Design of the “Q-Weak” Experimental Setup”, N. Simicevic, LATECH-CAPS-00-06a.
- [25] GEANT Detector Description and Simulation Tool, *CERN Program Library Long Writeup W5013*, CERN, Geneva, 1993
- [26] GEANT tutorial,  
[http://wwwinfo.cern.ch/asd/geant/tutorial/manual/tutorial\\_1.html](http://wwwinfo.cern.ch/asd/geant/tutorial/manual/tutorial_1.html)
- [27] “Toroidal Coil Magnet for the “Q-Weak” Experiment”, N. Simicevic, LATECH-CAPS-01-11a.
- [28] L. Harwood, private communication.
- [29] “Design of a Cerenkov Counter for the “Q-Weak” Experiment”, N. Simicevic, LATECH-CAPS-01-03a.
- [30] I. Adam *et al.* SLAC-PUB-7707, November 1997.
- [31] G. Rutledge and R. Michaels, “Systematics of  $Q^2$  for HAPPEX”, HAPPEX internal report, available at <http://www.jlab.org/rom> .
- [32] P. Degtiarenko, private communication.
- [33] M.J. Musolf, *et al.*, Phys. Rep. **239**, (1994) 1.

- [34] S.J. Dong, K.F. Liu, and A.G. Williams, Phys. Rev. D **58**, (1998) 074504.
- [35] K.A. Aniol, *et al.*, Phys. Lett. B **509**, (2001) 211.
- [36] TJNAF experiment E-99-115 (K.S. Kumar and D. Lhullier, spokespersons)
- [37] TJNAF experiment E-00-006 (D.H. Beck, spokesperson)
- [38] M.J. Musolf and B.R. Holstein, Phys. Lett. B **242**, (1990) 461.
- [39] S-L. Zhu, *et al.*, Phys. Rev. D **62**, (2000) 033008.
- [40] R. Hasty, *et al.*, Science **290**, (2000) 2021.
- [41] TJNAF experiment E-01-116 (D.H. Beck, spokesperson)
- [42] MIT-Bates experiment 00-04 (T. Ito, spokesperson)
- [43] This section is based on a  $Q_{weak}$  collaboration report (including figures) entitled “Asymmetry Contributions from the Aluminum End Windows in QWEAK”, M. Pitt, Virginia Tech, August 8, 2000.
- [44] T. Stovall, D. Vinciguerra, and M. Bernheim Nucl. Phys. A **91**, (1967) 513.
- [45] T.W. Donnelly, M.J. Musolf, W.M. Alberico, M.B. Barbaro, A. dePace, A. Molinari, Nucl. Phys. A **541**, (1992) 525.
- [46] E. Hadjimichael, G.I. Poulis, T.W. Donnelly, Phys. Rev. C **45**, (1992) 2666.
- [47] T.W. Donnelly, J. Dubach, I. Sick, Nucl. Phys. A **503**, (1989) 589.
- [48] TJNAF Experiment E-00-003, R. Michaels, P. Souder, G. Urciuoli, spokespersons.
- [49] K. Pomorski, P. Ring, G.A. Lalazissis, A. Baran, Z. Lojewski, B. Nerlo-Pomorska, M. Warda, Nucl. Phys. A **624**, (1997) 349.
- [50] W.M. Alberico, A. Molinari, page 389 of proceedings of the 1997 Paris Parity Violation Workshop
- [51] C.J. Horowitz, Phys. Rev. C **57**, (1998) 3430.
- [52] M. Hauger *et al.*, “A high-precision polarimeter”, NIM A461, 382 (2001), and nucl-ex/9910013.
- [53] Matt Poelker, injector group guru, private communication.
- [54] Maud Baylac, These du Diplome de Doctorat, “Mesure de la polarisation du faisceau d’electrons du Jefferson Laboratory par effet Compton pour l’experience de violation de parite HAPPEX en diffusion elastique electron-proton”, 2000, unpublished.

- [55] I. Passchier, C. W. de Jager, N. H. Papadakis, N. P. Vodinas, D. W. Higinbotham and B. E. Norum, “A Compton backscattering polarimeter for measuring longitudinal electron polarization,” Nucl. Instrum. Meth. A **414**, 446 (1998)
- [56] T. Pussieux, “The Compton Polarimeter for Jefferson Lab End Station A” (<http://www.jlab.org/compton/main.html>).
- [57] M. Baylac, *et al.*, “Mesure du temps de décroissance et de la photoluminescence des cristaux de PbWO<sub>4</sub> (English version)”, Internal Report DAPNIA-SPhN-97-47 (1997).
- [58] N.F. Mott, Proc. R. Soc. London, Ser. A **135**, (1932) 429.
- [59] S.P. Wells, *et al.*, Phys. Rev. C **63**, (2001) 064001.
- [60] D.T. Spayde, *et al.*, Phys. Rev. Lett. **84**, (2000) 1106.
- [61] Dave Gaskell, private communications.
- [62] R. David, M.Sc. thesis, Hampton University, 2000.
- [63] Particle Data Group: D. E. Groom *et al.* “Review of particle physics,” Eur. Phys. J. C **15**, 1 (2000).
- [64] M. J. Ramsey-Musolf, Phys. Rev. D **62**, 056009 (2000).
- [65] Y. Fukuda *et al.* [Super-Kamiokande Collaboration], Phys. Lett. B **433**, 9 (1998).
- [66] Q.R. Ahmad *et al.*, Phys. Rev. Lett. **87**, 071301 (2001).  
S. Fukuda *et al.*, Phys. Rev. Lett. **86**, 5651 (2001).
- [67] M. Cvetič and P. Langacker, “Z’ physics and supersymmetry,” e-print hep-ph/9707451.
- [68] J. E. Kim and H. P. Nilles, Phys. Lett. B **138**, 150 (1984).
- [69] J. Erler, Nucl. Phys. B **586**, 73 (2000).
- [70] CDF Collaboration: T. Affolder *et al.* Phys. Rev. Lett. **87**, 141802 (2001).
- [71] P. Langacker and M. Luo, Phys. Rev. D **45**, 278 (1992).
- [72] A. Kurylov and M. J. Ramsey-Musolf, “Charged current universality in the MSSM,” e-print hep-ph/0109222.
- [73] W. Buchmüller, R. Ruckl and D. Wyler, Phys. Lett. B **191**, 442 (1987) [Erratum-ibid. B **448**, 320 (1987)].
- [74] J.L. Hewett and T.G. Rizzo, Phys. Rev. **D56**, 5709 (1997).
- [75] P. Herzceg, private communication, to be published.

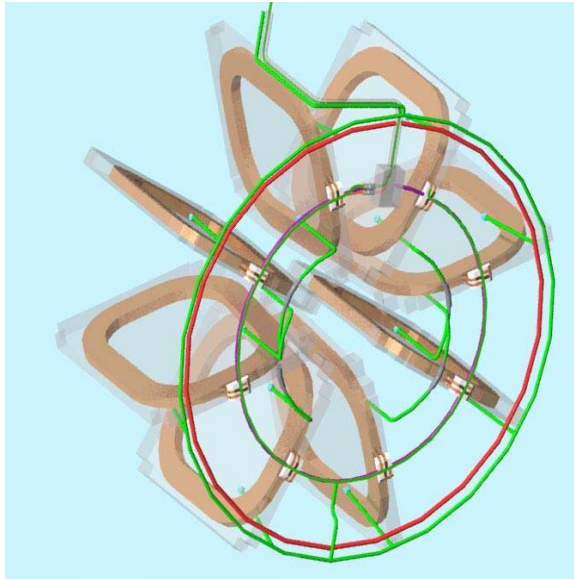


Figure 19: Inner structure of the  $G^0$  superconducting magnet system, showing eight superconducting coils and the liquid helium plumbing between them.

## A The $G^0$ Magnet Option

With some modification, the  $G^0$  Superconducting Magnet System (SMS) could be used for the measurement of the proton's weak charge. The  $G^0$  SMS consists of eight superconducting coils which generate the magnetic field that focuses scattered particles. This spectrometer has a field integral at maximum excitation of approximately 1.6 T-m. Because of their high specialization, the  $G^0$  detectors cannot be reused, and a new set of cryostat windows would have to be fabricated for both face plates. The cryogenic plumbing, seen in Figure 19, would also have to be rerouted.

Simulations were performed using parameters close to the reference design parameters in Table 1. [24] Elastic and inelastic electron tracks are shown in Figure 20, top and bottom, respectively. The elastic electrons are well-focused on the detector plane, while lower momentum electrons from inelastic processes are swept away.

Separation of elastic and inelastic events at the detector plane is shown in Figure 21.

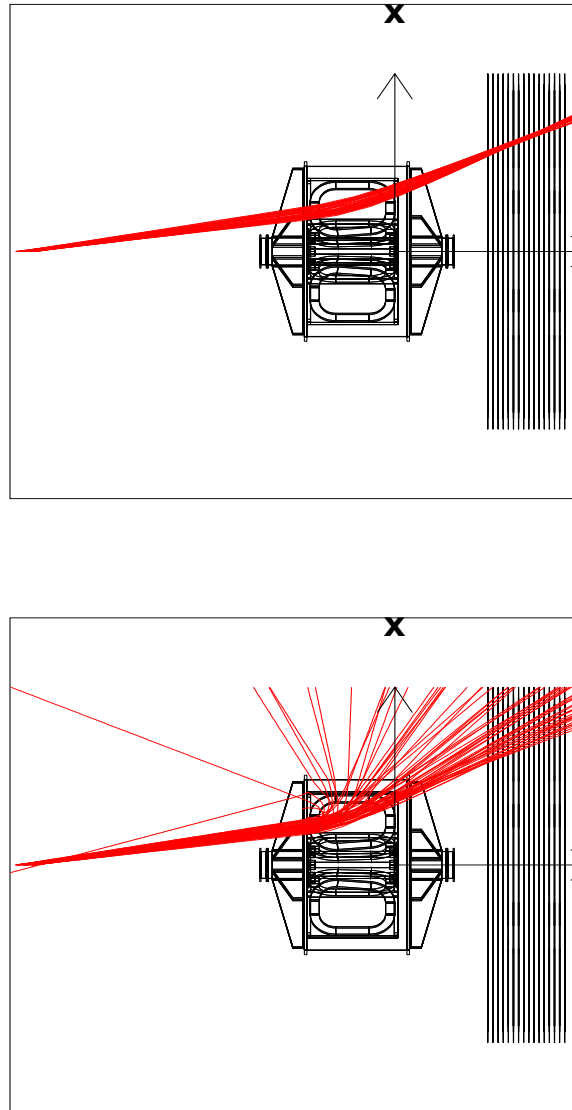


Figure 20: The side view of the test setup with a sample of elastic (top) and inelastic (bottom) trajectories restricted to  $\theta_e = 9.0 \pm 2$  deg and  $\phi_e = 0.0 \pm 15$  deg. The beam axis and direction is given by the horizontal arrow. The vertical arrow labeled X is a zero position along the beam axis in the standard  $G^0$  coordinate system.

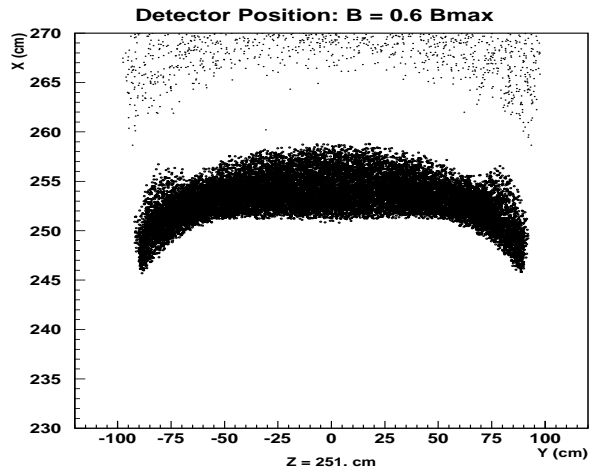


Figure 21: Separation of elastically (lower distribution) and inelastically (upper distribution) scattered electrons on selected detector position. The kinematics is restricted to  $\theta_e = 9.0 \pm 2$  deg and  $\phi_e = 0.0 \pm 15$  deg.

## B Physics Beyond the Standard Model

Any observed deviation of the renormalization group evolution (RGE) running of  $\sin^2 \theta_W$  from the Standard Model (SM) prediction could signal the presence of new physics, whereas agreement would place new constraints on possible SM extensions. There is little doubt that the SM will ultimately be embedded into a larger theory. Although the level of agreement between SM predictions and electroweak observables is impressive, the SM leaves open a number of conceptual questions. For example, it does not explain why electromagnetic charge is quantized, why parity and CP are violated (it merely parameterizes these symmetry violations), or why there exists such a disparity between the small electron mass and the large mass of the top quark. Similarly, the separation between the weak scale, associated with the breakdown  $SU(3)_c \times SU(2)_L \times U(1)_Y \rightarrow SU(3)_c \times U(1)_{EM}$ , and the Planck scale, where gravity becomes “strong”, is not protected against destabilizing SM radiative corrections.

A variety of scenarios for addressing these questions have been proposed, and a wide array of experimental tests of these ideas have been carried out. With the discovery of atmospheric and solar neutrino oscillations [65,66] (which are not explained by the SM), these searches have entered a new era. The deviations of precision electroweak observables from SM predictions may point to other effects of new physics. In addition to the deviations in the muon  $g - 2$ , DIS,  $\beta$ -decay, and APV, there are other ( $\lesssim 2\sigma$ ) deviations in the enhanced hadronic cross sections, both at the  $Z^0$  peak (LEP 1) and above the  $Z^0$  peak (LEP 2); in the value of  $M_W$ ; in the left-right asymmetry measured by the SLD Collaboration; and in the  $b\bar{b}$  production at LEP 2. Finally, there is a  $3\sigma$  discrepancy in the forward-backward asymmetry measured at LEP 1 [3].

When analyzing the sensitivity of  $Q_W^p$  to new physics, it is useful to identify the scales which characterize the SM and new physics contributions. The low-energy effective  $eq$  Lagrangian of the form  $A(e) \times V(q)$  is given by,

$$\mathcal{L} = \mathcal{L}_{SM}^{PV} + \mathcal{L}_{NEW}^{PV}, \quad (22)$$

where

$$\mathcal{L}_{SM}^{PV} = -\frac{G_F}{\sqrt{2}} \bar{e} \gamma_\mu \gamma_5 e \sum_q C_{1q} \bar{q} \gamma^\mu q, \quad (23)$$

$$\mathcal{L}_{NEW}^{PV} = \frac{g^2}{4\Lambda^2} \bar{e} \gamma_\mu \gamma_5 e \sum_f h_V^q \bar{q} \gamma^\mu q, \quad (24)$$

where  $g$ ,  $\Lambda$ , and the  $h_V^q$  are, respectively, the coupling constant, the mass scale, and effective coefficients associated with the new physics. The latter are in general of order unity; the explicit factor of 4 arises from the projection operators on left and right (or vector and axial-vector) chiral fermions. In the same normalization, the SM coefficients take the values  $C_{1u}/2 = -0.09435 \pm 0.00011$  and  $C_{1d}/2 = +0.17068 \pm 0.00008$  [63], for up and down quarks, respectively, and one can write,

$$Q_W^p(\text{SM}) = -2(2C_{1u} + C_{1d}) \approx 0.0721 \quad (25)$$

Thus, a 4% measurement,  $\Delta Q_W^p = \pm 0.0029$ , would test new physics scales up to

$$\frac{\Lambda}{g} \sim \frac{1}{\sqrt{\sqrt{2}G_F|\Delta Q_W^p|}} \approx 4.6 \text{ TeV}. \quad (26)$$

The sensitivity to non-perturbative theories (such as technicolor and other strong coupling dynamics) with  $g \sim 2\pi$  could even reach  $\Lambda \approx 29$  TeV.

Before considering the implications for particular models of new physics, it is instructive to consider the model independent implications of a 4%  $Q_W^p$  measurement. In Fig. 2, we plot the present constraints on  $\Delta C_{1u}$  and  $\Delta C_{1d}$ , the shifts in the  $C_{1q}$  caused by new physics. In terms of the interactions in  $\mathcal{L}_{NEW}^{PV}$ , one has

$$\Delta C_{1q} = -\frac{\sqrt{2}}{4G_F} \frac{g^2}{\Lambda^2} h_V^q \approx -0.03 \left( \frac{g}{\Lambda/\text{TeV}} \right)^2 h_V^q \quad . \quad (27)$$

These constraints are derived from the Cesium weak charge results, the MIT-Bates  $^{12}\text{C}$  and SLAC Deuterium parity violation measurements. As long as  $h_V^u$  and  $h_V^d$  are almost perfectly correlated, only an extremely weak limit on the mass-to-coupling ratio  $\Lambda/g$  can be derived from the data. The result is an elongated ellipse. The impact of the proposed  $Q_W^p$  measurement is indicated by the smaller ellipse, assuming the experimental central value equals the SM prediction. Because the  $Q_{weak}$  experiment is a precise measurement which is sensitive to a different linear combination of  $C_{1u}$  and  $C_{1d}$  than the earlier measurements, the reduction in allowed phase space is dramatic.

While limits within particular models may vary from this value (for a recent review, see Ref. [14]), this model independent analysis illustrates the decisive role a  $Q_W^p$  measurement could play. For example, a particularly well-motivated class of new physics models predict the existence of extra TeV scale  $Z'$  bosons. In the simplest models based on Grand Unified Theories (GUT) one expects  $g \sim 0.45$ , so that one can study  $Z'$  bosons (with unit charges) up to  $M_{Z'} \approx 2.1$  TeV.  $Z'$  bosons are predicted in very many extensions of the SM ranging from the more classical GUT and technicolor models to supersymmetry and string theories. We discuss the sensitivity of  $Q_W^p$  to  $Z'$  bosons, as well as other scenarios, below.

## B.1 Extra Neutral Gauge Interactions

The introduction of neutral gauge symmetries beyond those associated with the photon and the  $Z^0$  boson have long been considered as one of the best motivated extensions of the SM. In the context of supersymmetry, they do not spoil the approximate gauge coupling unification predicted by the simplest and most economic SUSY scenarios. Moreover, in many SUSY models (though not the simplest  $SO(10)$  ones), the additional  $U(1)'$  gauge symmetry forbids an elementary bilinear Higgs  $\mu$ -term, while allowing an effective  $\mu$  to be generated at the scale of  $U(1)'$  breaking without introducing cosmological problems [67]. In various string-motivated models of radiative breaking, this scale is comparable to the electroweak scale (*i.e.*, less than a TeV) [67], thereby providing a solution to the  $\mu$ -problem [68] and enhancing the prospects that a  $Z'$  could be detected in collider experiments or seen indirectly via precision electroweak data. An extra  $U(1)'$  symmetry could also explain proton stability, which is not automatic in supersymmetric models, or it could solve both, the  $\mu$  and proton lifetime problems, *simultaneously* [69].

From a phenomenological standpoint, direct searches at the Tevatron [17] have as yet yielded no evidence<sup>5</sup> for the existence of the extra neutral  $Z'$  boson associated with the  $U(1)'$ , providing

---

<sup>5</sup>See, however, Ref. [70] which reports a  $2\sigma$  deficit in the highest mass bin of the leptonic forward-backward b quark asymmetry seen by the CDF Collaboration.

instead only lower bounds of about 600 GeV (depending on the precise nature of the  $Z'$ ).

On the other hand, several indirect effects could be attributed to a  $Z'$ . The  $Z^0$  lineshape fit at LEP [3] yields a significantly larger value for the hadronic peak cross section,  $\sigma_{\text{had}}$ , than is predicted in the SM. This implies, *e.g.*, that the effective number of massless neutrinos  $N_\nu$  is  $2.986 \pm 0.008$ , which is roughly  $2\sigma$  lower than the SM prediction,  $N_\nu = 3$ . As a consequence, the  $Z^0$ -pole data currently favors  $Z'$  scenarios with a small amount of  $Z^0$ - $Z'$ -mixing which mimics a negative contribution to the invisible  $Z^0$  decay width. The most recent results in APV can be easily explained if one assumes that  $Z'$  exchange decreases the SM  $Z^0$  boson contribution. Finally, the result by the NuTeV Collaboration [11] can be brought into better agreement when one allows a  $Z'$ . Although the improvement is modest, it is non-trivial, since the deviations in the weak mixing angles derived from NuTeV and APV show opposite signs, but can nevertheless both be improved by assuming  $Z'$  effects.

In analyzing the impact of a  $Z'$  on  $Q_W^p$ , we employ Eq. (24) with  $\Lambda = M_{Z'}$  and  $g = g_{Z'} = \sqrt{5/3} \sin \theta_W \sqrt{\lambda} g_Z$  [71], with  $\lambda = 1$  in the simplest models.  $g_Z^2 = 8G_F M_Z^2 / \sqrt{2}$  is the SM coupling constant for the ordinary  $Z^0$ . Consider the Abelian subgroups of  $E_6$ ,

$$E_6 \rightarrow SO(10) \times U(1)_\psi \rightarrow SU(5) \times U(1)_\chi \times U(1)_\psi \rightarrow SU(3)_C \times SU(2)_L \times U(1)_Y \times U(1)_\chi \times U(1)_\psi.$$

Then, the  $Z'$  can be written as the linear combination,

$$Z' \sim -\cos \alpha \cos \beta Z_\chi + \sin \alpha \cos \beta Z_Y - \sin \beta Z_\psi. \quad (28)$$

Considerations of gauge anomaly cancellation and the  $\mu$  and proton lifetime problems in SUSY models mentioned earlier, also favor a  $Z'$  of that type [69]. The assignment of SM fermions to representations of  $SO(10)$  implies that the  $Z_\psi$  has only axial-vector couplings and can generate no PV  $e$ - $f$  interactions of the type in Eq. (24), whereas the  $Z_\chi$  generates only PV  $e$ - $d$  and  $e$ - $e$  interactions of this type. In fact, in this class of models the weak charges of the proton and the electron have equal magnitude. Thus, should the measurement proposed here show a deviation from the SM prediction, a comparison with the SLAC-E-158 experiment measuring the electron's weak charge would be a powerful way to discriminate between this class of models and other SM extensions.

Presently, a global fit to all precision observables within the SM yields an overall  $\chi^2/\text{d.o.f.}$  of 54.8/41 ( $M_H = 115$  GeV). Including a 600 GeV  $Z'$  and allowing  $\alpha$ ,  $\beta$ , and the  $Z^0$ - $Z'$ -mixing parameter,  $\theta$ , improves the goodness of the fit significantly,  $\chi^2/\text{d.o.f.} = 49.2/38$ . The probability to get an improvement of this magnitude or larger due to a statistical fluctuation is only 13%. Thus, the present data is better described with an extra neutral gauge boson than without. Clearly, more experimental information is needed before a firm conclusion is possible.

To study the impact of a  $Z'$  on  $Q_W^p$  we consider the current best fit values,  $\alpha = -0.8_{-0.8}^{+1.2}$ ,  $\beta = 1.2_{-0.4}^{+0.2}$ , and  $\sin \theta = 0.0009_{-0.0006}^{+0.0007}$ , obtained for  $\lambda = 1$ . In this case,  $Q_W^p = 0.0780$  is predicted, that is a  $+2\sigma$  effect. If the physical value of  $Q_W(\text{Cs})$  is at the lower end of its  $1\sigma$  allowed range, the best prediction would be  $Q_W^p = 0.0810$ , which is  $+3.1\sigma$  above the SM expectation.

Thus, one of the most straightforward and best motivated extensions of the SM describes the current data better than the SM itself and predicts a significant deviation in  $Q_W^p$ . In view of the very high precision and very high energy measurements at the  $Z^0$  factories LEP and SLC, it is

quite remarkable that a 4% measurement at very low  $Q^2$  and operating with a several orders of magnitude lower budget offers a more sensitive probe of TeV scale physics. If the SLAC-E-158 and  $Q_W^p$  measurements would show results consistent with a  $Z'$  and with each other, they could be combined, offering strong evidence for the new force.

Even if a  $Z'$  is detected at the Tevatron or the LHC first, it will be important to constrain its properties. Its mass will be measured in course of the discovery, and  $\sin\theta$  is mainly constrained by LEP 2. The  $U(1)'$  charges and the couplings to quarks and leptons, however, are best determined by low-energy precision measurements. The allowed regions of the parameters  $\alpha$  and  $\beta$  of the case above can be decreased by 40%. For example, if  $Q_W^p$  is found  $3\sigma$  above the SM prediction, the parameter  $\alpha$  would be significantly different from zero, while a  $4\sigma$  effect would establish the mixing with hypercharge with more than 90% confidence. Again, even more detailed information can be obtained when the SLAC-E-158 result is also used.

## B.2 Supersymmetry

Supersymmetry (SUSY) has long been considered a likely ingredient of an “extended” Standard Model. The theoretical motivation includes superstring theories, for which the existence of low-energy SUSY is a prediction; resolution of the “hierarchy problem” associated with Higgs mass renormalization and stability of the weak scale without resorting to fine tuning of parameters; and gauge coupling unification at the GUT scale. From a phenomenological standpoint, the recently reported deviation of the muon anomaly from the Standard Model prediction provides a tantalizing hint of SUSY, since contributions from “superpartner” loops provide a natural explanation for the effect.

The detailed way in which low-energy SUSY becomes manifest remains an open question. Since no superpartners have yet been seen in direct search measurements, their masses must be split from those of the Standard Model particles, thus implying some break down of exact SUSY. There exists a theoretical bias that SUSY breaking occurs at some high scale in a “hidden” sector and that its effects are transferred to low-energy phenomena via new gravitational or gauge interactions. These models of gravity or gauge mediated SUSY breaking make strong predictions for superpartner mass hierarchies. Low-energy charged current data, on the other hand, are not consistent with these predictions unless a symmetry known as “R parity” is violated[72,64]. This symmetry is equivalent to conservation of baryon minus lepton number, and its violation implies the nonconservation of either B and/or L.

In order to evade present limits on proton decay, one typically sets  $\Delta B \neq 0$  R parity violating (RPV) interactions to zero, leaving only  $\Delta L \neq 0$  effects. Two types of L-violating RPV interactions occur: those which are purely leptonic, involving the exchange of “sleptons” (Fig. 22a), and semileptonic interactions arising from “squark” exchange (Fig. 22b). We denote corrections induced by purely leptonic interactions as  $\Delta_{ijk}$  and those arising from the semileptonic effects as  $\Delta'_{ijk}$ , where the indices refer to different generations. Low-energy observables are sensitive to both types of corrections. The dependence of semileptonic observables on  $\Delta_{ijk}$  arises from the normalization of amplitudes in terms of the muon decay Fermi constant and from the definition of the weak mixing angle.

In Fig. 23, we plot the present constraints relevant to charged and neutral current interactions

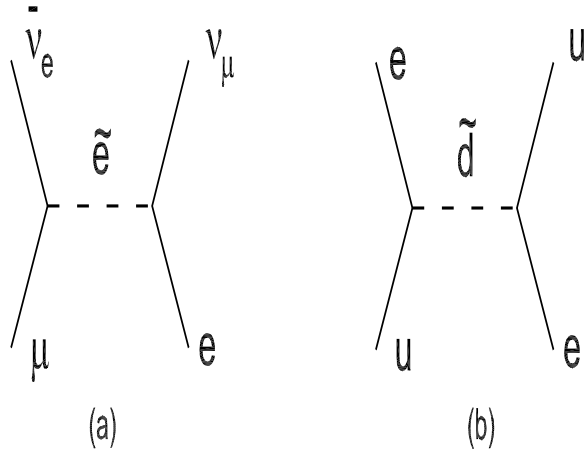


Figure 22: Slepton and squark exchange contributions to muon decay (a) and eq interactions (b) arising in R parity violating SUSY models.

of light quarks and leptons. The 90% C.L. contour is dominated by the results of superallowed nuclear  $\beta$ -decays and the requirement of CKM unitarity. Additional input is obtained from the Cesium weak charge, the leptonic ratio for  $\pi$  decay, and measurements of the  $W$  mass. The present data could accommodate a +9% (+10%) shift in  $Q_W^p$  at 90% (95%) C.L. The prospective impact of the proposed  $Q_W^p$  measurement is shown by the dotted ellipse in Fig. 23a and 23b. For case (a), we assume the experimental central value coincides with the SM prediction for  $Q_W^p$ . In Fig. 23b, we assume the central value comes below the SM prediction by two standard deviations.

Depending on the outcome of the proposed measurement, the impact on this new physics could be severe. At present SUSY provides one of the only simultaneous explanations of both the charged current and neutral current low-energy deviations from the SM (superallowed  $\beta$ -decay and Cesium atomic PV, respectively). The  $Q_W^p$  measurement would provide an important diagnostic as to whether this solution remains a viable one. In contrast, the prospective impact of the PV Møller asymmetry measurement on the plots in Fig. 23 is less pronounced, since it competes directly with  $W$ -mass measurements, whose effects are already included in the fit. A comparison of  $Q_W^p$  and Møller results, however, could provide additional information. For example, were both measurements to agree with each other, but not with the SM, it would be unlikely that RPV SUSY interactions were responsible for the effect.

### B.3 Leptoquarks

Leptoquarks – bosons which have both nonzero baryon number  $B$  and lepton number  $L$  – have long been a popular, though somewhat exotic, candidate for new physics. In leptoquark models consistent with the  $SU(3)_c \times S(2)_L \times U(1)_Y$  symmetry of the SM [73,74], they can give rise to new tree-level, parity violating  $e - q$  interactions, as illustrated in Fig. 24. Theoretically, spin-1 (vector) leptoquarks arise naturally in models of extended gauge symmetry, where they correspond

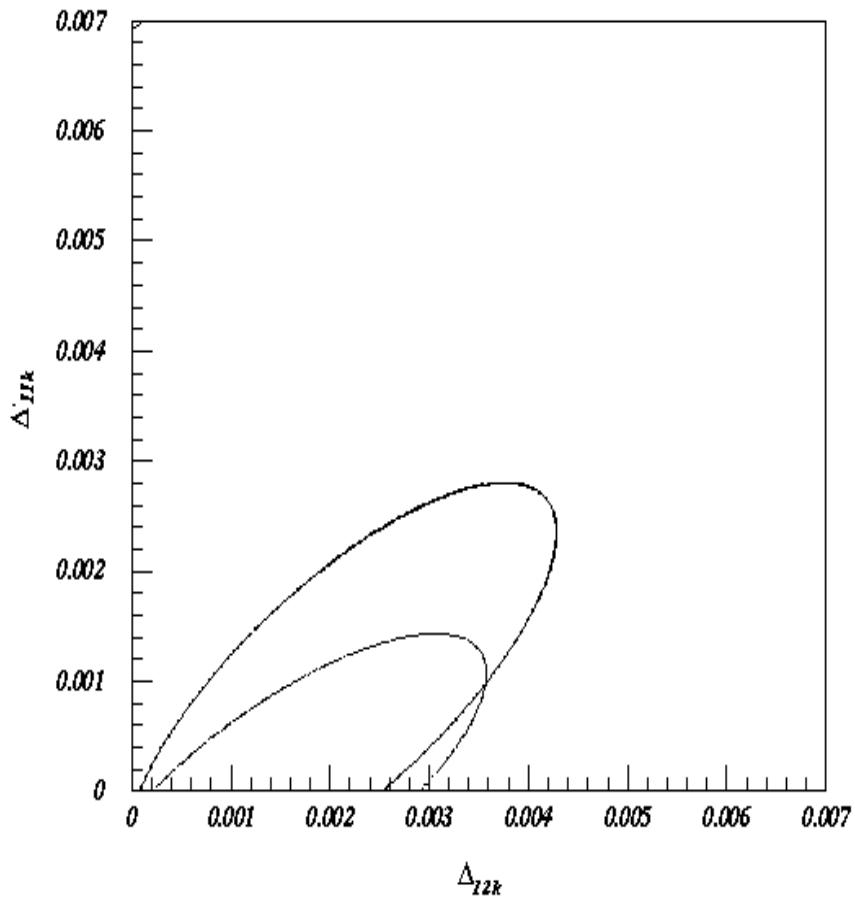


Figure 23: Present and prospective 90% constraints on RPV SUSY corrections. The solid ellipse denotes present constraints from charged and neutral current data. The dashed ellipse indicates impact of the proposed  $Q_W^p$  measurement. An experimental central value equal to the SM prediction for  $Q_W^p$  is assumed.

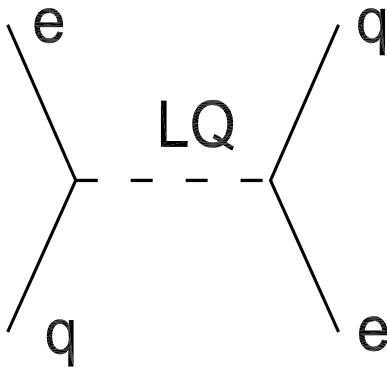


Figure 24: Leptoquark (LQ) exchange contributions to parity violating  $eq$  interaction.

to additional gauge bosons required by gauge invariance. Scalar leptoquarks occur naturally in RPV SUSY models, where they coincide with the exchanged squarks of Fig. 24<sup>6</sup>. Thus, it is useful to consider the prospective impact of the  $Q_W^p$  on leptoquark models.

The implications of electroweak data for scalar leptoquark models have been analyzed most recently in Refs. [18,19]. Included in those analyses are data from deep inelastic neutral current scattering at HERA, Drell-Yan dilepton production at the Tevatron, hadronic cross sections at LEP 2, neutrino-nucleus deep inelastic scattering, light quark  $\beta$ -decay, atomic parity violation, and the SLAC, Mainz, and MIT-Bates parity violating electron scattering experiments. At the time of Ref. [18], the Cesium weak charge was believed to deviate from the SM by  $2.3\sigma$ . The analysis of Ref. [19], in contrast, was performed after inclusion of Breit corrections moved the Cesium result into agreement with the SM. In light of the recent variations in atomic theory, it is useful to consider  $Q_W^p$  in light of both analyses.

In the analysis of Ref. [18] ( $2.3\sigma$  deviation for Cesium), two species of leptoquarks were found to provide an explanation for the effect while maintaining consistency with all other electroweak data:  $R_2^R$  and  $\vec{S}_3$  (in the notation of Ref. [74]). While the effects of the Cesium result were not included in a global fit, one can estimate the prospective impact of  $R_2^R$  and  $\vec{S}_3$  on  $Q_W^p$ . Were either of these leptoquarks to account for a  $2.3\sigma$  deviation of Cesium from the SM value, they would each produce a 10% shift in  $Q_W^p$ , respectively. The same leptoquarks could also produce significant deviations of  $Q_W^p$  from the SM prediction even if the Cesium weak charge is taken to agree with the SM as assumed in Ref. [19]. The corresponding expectation is shown in column of Table I. Under either scenario, one could anticipate sizeable effects in  $Q_W^p$  if low-energy leptoquarks constitute part of an extended Standard Model.

No recent, comparable analysis of vector leptoquark contributions has been published. An analysis by Herczeg, however, is in process[75], though the results were not available at the time this proposal was submitted.

We note that, as in the case of other scenarios discussed above, the comparison of a  $Q_W^p$  measurement with results of the Møller parity violation experiment provides a powerful diagnostic.

<sup>6</sup>Technically speaking, the squarks in Fig. 24 are not leptoquarks, since they do not carry lepton number. However, their effects are indistinguishable from scalar leptoquark exchange.

LQ Species	$\Delta Q_W(p)/Q_W(p)$
$S_1^L$	0.04
$S_1^R$	-0.07
$\tilde{S}_1$	-0.05
$\vec{S}_3$	0.14
$R_2^L$	-0.10
$R_2^R$	0.14
$\tilde{R}_2$	-0.04

Table 9: Prospective impact of scalar leptoquark interactions on  $Q_W^p$ . First column indicates species, according to the notation of Ref. [74]. Second column gives maximum allowed shift in  $Q_W^p$  assuming agreement between the Cesium weak charge and the SM (Ref. [19]).

Leptoquark effects enter parity violating Møller scattering only at loop level, and their effects are considerably smaller than the anticipated precision of the E-158 measurement [14]. Thus, should both experiments deviate from the SM prediction by two or more standard deviations, one would suspect the effect was not generated by leptoquarks. On the other hand, a deviation of  $Q_W^p$  of the scale indicated by the entries in Table 9, coupled with the absence of any deviation in the Møller measurement, could point toward leptoquark interactions.

## C Miscellaneous Administrative Limits

### C.1 Beam Dump Current Density Limit

JLab imposes a beam current limit of  $12 \mu\text{A}/\text{cm}^2$  at the face of the beam dump for all experiments (the ‘‘Sinclair limit’’). In order to check whether this limit would interfere with the  $180 \mu\text{A}$  beam current we propose to use, we consider the effects of multiple scattering in some of the beam-line elements. The rms multiple scattering angle encountered by a beam of momentum  $p$  after traversing a thickness  $x$  of material characterized by a radiation length  $X_0$  is  $\theta_0 = \frac{13.6 \text{ MeV}}{p\beta} \sqrt{x/X_0}(1 + .038 \ln(x/X_0))$ . Over a distance  $z$  to the dump, the rms deflection in the plane of the dump corresponding to this multiple scattering angle is  $y_{plane}^{rms} = \frac{1}{\sqrt{3}}z\theta_0$ .

In our case,  $p \simeq 1 \text{ GeV}/c$  and  $\beta = 1$ . The contributions from various multiple scattering sources is summarized in Table 10. From this table we see that the  $12\mu\text{A}/\text{cm}^2$  beam dump current limit is not a problem for this experiment, even without rastering. In fact, the existing diffuser at the mid-point of the beam dumpline provides enough diffusion by itself to permit currents up to  $200\mu\text{A}$ .

Item	dx to dump z(m)	$\bar{X}_0$ cm	x cm	$\theta_0$ mrad	y mm	Individual $I_{max}$ $\mu\text{A}$	Cumulative $I_{max}$ $\mu\text{A}$
Diffuser	12.3	35.6	1’’	3.3	23.2	203	203
Dump window	24.3	8.9	0.02	0.5	7.0	18	<b>343</b>
Target windows	32	8.9	0.01’’	0.6	10.4	41	621
Helium in upstream half of dumpline	18	$5.2 \times 10^5$	1190	0.5	5.2	10	790
$LH_2$	32	866	35	2.4	44	741	3064
$2 \times 2 \text{ mm}^2$ raster					$\pm 4$	8	3341

Table 10: Calculation of our beam current limits, assuming the ‘‘Sinclair current density limit’’ of  $12 \mu\text{A}/\text{cm}^2$ , a beam energy of  $\simeq 1 \text{ (GeV}/c)$ , and the expected materials in our beamline. In the worst case scenario of no raster and no target, the maximum current would be  $343 \mu\text{A}$  which is almost a factor of 2 larger than our proposed production current of  $180 \mu\text{A}$ .

### C.2 Site Boundary Dose

The JLab limit for the site boundary dose is  $10 \text{ mRem}/\text{year}$ , or 10% of the DOE limit. To put this number in perspective, natural background is approximately  $300 \text{ mRem}/\text{year}$ , hence the JLab limit is only 3% of the natural background level. It is therefore not surprising that estimation of the site boundary dose is a routine part of submitting a JLab beam scheduling request.

The proposed target radiation length (4%) and the proposed current of  $180 \mu\text{A}$  are each about a factor of two larger than the running conditions of the Madey/Kowalski  $G_E^n$  experiment which ran in Hall C in 2000-2001. Thus if there were no mitigating circumstances, the site boundary

dose rate for the  $Q_{weak}$  experiment could be expected to be roughly 4 times larger than than in the Madey/Kowalski experiment for roughly the same beam energy. Using site boundary data provided by the Radiation Control group [32], and attributing half the dose to simultaneous high luminosity Hall A operations, a reasonable estimate for the Madey/Kowalski experiment site boundary dose rate is 0.8 mRem per 1000 hours of floor time. Our estimated dose rate for a 2000 hour  $Q_{weak}$  run, assuming twice as many hours of floor time, is therefore  $0.8 \times 4 \times 2 = 6.4$  mRem, or 64% of the JLab limit (or 2% above the natural background level).<sup>7</sup> This unrealistically assumes our experiment would take 2000 hours of beam time in a single calendar year, but provides an upper estimate. In order to stay well below the JLab limit, and to permit other high luminosity experiments to run the same year, one would like to reduce this naive dose estimate by a factor of 2.

GEANT simulations by the Radiation Control group typically show that the site boundary dose due to Hall C operations is dominated by high energy neutrons which leave the target at small vertical angles, pass through the base of the dome and earth berm, enter the atmosphere, and are subsequently downscattered to the site boundary (*ie*, skyshine). The beam dump makes a relatively small contribution. Thus, luminosity in the Hall, rather than total current, is the source term. Knowing this immediately suggests that the  $Q_{weak}$  experiment will have three important mitigating conditions:

- Except for particles scattered into the solid angle of interest, the remaining forward scattered particles will encounter heavy metal collimators.
- The  $Q_{weak}$  target will be located significantly downstream of the standard Hall pivot. Thus a larger fraction of the beam scattered to small angles will be captured by the beam dump line, and the neutrons which do exit the dome will do so at larger average scattering angle.
- The production target will be Hydrogen rather than Deuterium as was used in the Madey/Kowalski experiment.

If, despite these mitigating conditions, RadCon GEANT simulations of the  $Q_{weak}$  experiment suggest that the basic design of the experiment still produces too large a fraction of the site boundary dose (and we emphasize that we are still talking about a very small fraction of the natural background dose), then additional skyshine shielding can be emplaced before or after the top of the collimator. For example, the addition of 5 cm of lead (the thickness of a brick) can be expected to reduce the flux of high energy neutrons by a factor of 2.

### C.3 Beam Containment Policy Current Limit

During early operations at JLab, the easiest way to implement protection for the 1 MWatt beam dumps in Hall A and C was to hardware-limit the Hall currents each to 180  $\mu$ A. For example, assuming 5-pass beam at 5.56 GeV, then 180  $\mu$ A would correspond to 1.0 MWatts. However, since the  $Q_{weak}$  experiment employs a beam energy of only 1.165 GeV, the beam power dissipated

---

<sup>7</sup>This is a working estimate by our collaboration and not by the Radiation Control group. When the experiment parameters are finalized we will consult with RadCon to get a firmer estimate and discuss mitigation if necessary.

in the dump will be only 210 kWatts. There is clearly no threat from our experiment to the dump due to total power dissipation, nor due to the dump window current density limit which was examined above.

In order for the  $Q_{weak}$  experiment to run reliably near  $180 \mu\text{A}$ , the Hall C current limit would have to be raised slightly. Of course, if we are only permitted to receive  $170 \mu\text{A}$ , for example, the target length could be increased a few cm to keep the luminosity constant.

#### **C.4 Physics Division Administrative Limit**

There is also a Physics Division Administrative limit of about  $120 \mu\text{A}$  which would be waived by Larry Cardman for experiments which make a sufficiently compelling physics case. This limit is put in place to simplify the routine scheduling of multiple high current, high beam energy experiments.

## D Window Backgrounds

### Elastic scattering from target windows:

Despite the fact that the contribution of the elastic scattering on the aluminum nucleus to the overall rate is small (1.1%), the effective contribution to the asymmetry is significant because the asymmetry from elastic scattering on aluminum is 10 times larger. This comes from the difference in the couplings:  $(1 - 4 \sin^2 \theta_W)$  for elastic scattering on the proton versus  $4 \sin^2 \theta_W$  for elastic scattering on the aluminum nucleus. It is worth noting up front that an alternate solution for this background is to select a window material in which the effects discussed below become essentially negligible. Specifically, if the target windows were to be made of Beryllium then this background would become quite small. This option is under study, but will not be addressed further at this point. The question for now is, what is the error on the theoretical estimate of the Aluminum asymmetry?

The expression for the asymmetry can be written as [47]:

$$A = \frac{G_F Q^2}{4\pi\alpha\sqrt{2}} \left[ 1 - 4 \sin^2 \theta_W - \frac{F_n(Q^2)}{F_p(Q^2)} + \Gamma(Q^2) \right] \quad (29)$$

where

$$F_{p,n}(Q^2) = \frac{1}{4\pi} \int d^3r j_0(Qr) \rho_{p,n}(r) \quad (30)$$

are the Fourier transforms of the proton and neutron densities. (We use the form factor  $F(Q^2 = 0.03 \text{ GeV}^2) = 0.27$  from [44].) There will be some uncertainty in the asymmetry due to lack of knowledge of the ratio  $F_n/F_p$ . For example, reference [49] observes differences of about 0.1 fm in the proton and neutron radii in  $^{27}\text{Al}$  for different choices of parameters in a mean field model. This would correspond to about a 3% uncertainty in the neutron radius.

The more significant factor is the  $\Gamma(Q)$  factor in the above equation. This represents deviations from the ideal expression due to nuclear structure effects such as isospin breaking [47,50] and Coulomb distortions [51]. At the  $Q_{weak}$  q value ( $0.9 \text{ fm}^{-1}$ ) this factor (for the nearest calculated nucleus,  $^{30}\text{Si}$ ) varies from 0.8% to 4% depending on the shell-model space used. So we assign an uncertainty of  $\simeq 4\%$ .

Finally, the expression in Equation 29 is only strictly true for a spin 0 nucleus (*ie* charge scattering only). The asymmetry for  $^{27}\text{Al}$  (spin 5/2) will contain contributions from higher multipoles as well. Fairly general expressions exist in the literature [21] from which it could presumably be derived.

Given the above uncertainties, a conservative estimate of the error bar for a theoretical calculation of this asymmetry might be about 10%, implying a 1.1% systematic error *assuming no dedicated window background measurement*.

### Quasielastic scattering from windows:

For the quasielastic entries in Table 1, it was assumed that the asymmetries for the proton and neutron in aluminum are the same as the free proton and neutron. There are of course nuclear corrections to this. Parity-violating quasielastic electron scattering was considered in a general survey article in [45]. They did not consider the final state interactions in detail.

These effects have been calculated by Hadjimichael *et al* [46] in detail for deuterium. Generally, they find that the deviations from the simple picture become small ( $\sim 1\text{-}2\%$ ) for large  $q$  ( $> 400$  MeV/c) and backward angle running. From a figure in their paper chosen to be as near to the  $Q_{weak}$  kinematics as possible ( $q=173$  MeV/c,  $\theta = 9^\circ$ ), one finds that the difference between the asymmetry derived in a realistic final state interaction (FSI) calculation (about 0.9 ppm) and the simple picture of free proton and neutron (about 0.33 ppm) is a factor of  $\simeq 3$ . The good news is that the model dependence of the FSI calculation from using very different N-N potentials is only at the 10% level.

The collaboration is exploring developing a more precise calculation of this asymmetry. For example, if the asymmetry really changed by an extreme amount say a factor of 3, then the proton contribution in our experiment would go from 1.1% to 3.3%. However, if the modeling of this asymmetry can be believed even at the 10% level, then the systematic error associated with this *assuming no dedicated window background measurement* would only be 0.3%.